PB-228 047

FACTORS INFLUENCING STREAM TEMPERATURES

John Seaders

Oregon State University
Corvallis, Oregon

1 August 1968

DISTRIBUTED BY:

NTIS

National Technical Information Service
U. S. DEPARTMENT OF COMMERCE
5285 Port Royal Road, Springfield Va. 22151

051206

PB 228 047

Final Report Part II

FACTORS INFLUENCING STREAM TEMPERATURES

Federal Water Pollution Control Administration

Department of the Interior

Division of Water Supply and Pollution Control

Research and Training Grants Branch

Research Grant WP 00684-01, 02, 03

Reproduced from best available copy.

Investigator

John Seaders
Associate Professor
Department of Civil
Engineering

Oregon State University
Engineering Experiment Station
Corvallis, Oregon

August 1, 1968

Reproduced by
NATIONAL TECHNICAL
INFORMATION SERVICE
U S Department of Commerce
Springfield VA 22151

TABLE OF CONTENTS

	Page
INTRODUCTION	1
SCOPE AND PURPOSE	2
ANALOG TERRAIN MODEL	3
Radiation Exchange	3
View factors	6
Analog Circuits	13
Examples and Solution of Analog Model	15
Other Methods for View Factor Evaluation	19
Prototype Fieldstudy	21
Equipment for Observations and Data Presentation Rogue and Deschutes River Sites	21
Discussion of Results	35
Conclusions	43
FIELD GEOMETRY AND SHADING EFFECTS	44
Solar Radiation Rates and Quantities	44
Relationships between Solar Radiation, Exposure Position and Shading of Terrain Equation Development	50
Analog Model of Shading and Solar Radiation	54
Application of Theory to Deschutes River	61
CONCLUSIONS	66
APPENDICES	
A Integration of View Factor Functions	67
B Terrain Data Used in Calculating the Values of fig's. 23 and 24	69
C Verification of Analog Model with General Equation for Shading Angle	71
D Accumulated Solar Radiation Received at a Horixontal Surface as a Function of Time, Latitude, and Solar Altitude	74
E Solar Radiation Blocking by Terrain Calculation for Deschutes River--Comparison of Sections Sinomox Quadrangle	77
BIBLIOGRAPHY	80

LIST OF FIGURES

Figure		Page
1	Nomenclature for Intensity of Radiation	4
2	View Factor Reduction by Obstruction	8
3	Graphical Presentation of View Factor	9
4	Radiation Exchange between Infinite Surfaces	11
5	Radiation Exchange between Finite Surfaces	12
6	Analog Circuit Representing Radiation Exchange between Finite Surfaces	12
7	Simplified Analog Circuit of Radiation Exchange between Infinite Surfaces	14
8	View Factor Analysis of a Parallel Plane	19
9	Barnes IT-3 Mounted on top of Transit on Operation on Rogue River Site #3	21
10	I R Thermometer--Trace of Terrain Temperature Obtained with XY Recorder	23
11	I R Thermometer--Trace of Terrain Temperature Obtained with XY Recorder	24
12	Horizon Trace of Deschutes River Site #1	26
13	Map of Lower Rogue River Area	29
14	Map of Deschutes River Area	30
15	Photograph of Rogue River Site #1	31
16	Photograph of Rogue River Site #1	31
17	Photograph of Rogue River Site #2	32
18	Photograph of Deschutes River Site #1	32
19	Photograph of Deschutes River Site #1	33
20	Photograph of Deschutes River Site #2	33
21	Correlation Curves of Kipp Solarimeter with ENR	36

Figure		Page
22	Rogue River Site #1--Radiant Heat Exchange Curves	37
23	β Atmospheric Radiation Factor	39
24	Deschutes River Site #1--Radiant Heat Exchange Curves	41
25	Effect of Cloud Cover on Insolation	48
26	Effect of Solar Altitude and Cloud Cover on Reflectivity	48
27	Net Radiation Received on a Horizontal Surface as a function of Solar Altitude	49
28	Geometry of Terrain Shading in NE Quadrant	50
29	Geometry of Terrain Shading in NW Quadrant	52
30	Analog Terrain Shading Model	55
31	Shading Angle for "Lat. 45°" as a function of α and β for 1 July and 1 August	57
32	Shading Angle for "Lat. 45°" as a function of α and β for 16 August and 23 September	58
33	Length of Solar Day as a function of Latitude and Dates	60
34	Accumulated Solar Radiation for Latitude 45° N	62
35	Solar Radiation Trace from Kipp Solarimeter showing Radiation Blocking by Terrain	63
36	Section of Deschutes River Sinomox Quadrant ($7\frac{1}{2}$")	64
37	Section of Deschutes River Sinomox Quadrant ($7\frac{1}{2}$")	65

LIST OF TABLES

Table		Page
1	Radiation of Atmosphere or Water to Environment at Absolute Zero	16
2	View Factor Calculations for Deschutes Site No. 1	27
3	Rogue River Terrain Temperatures	34
4	Deschutes River Terrain Temperatures	34
5	Average Solar Radiation Values in the United States	44
6	Extra Terrestrial Intensity on a Surface	46
7	Solar Radiation for Clear Atmosphere	46
8	Length of Solar Day for Dates and Latitudes	59

v.

STREAM HEATING FROM TERRAIN SOURCES

INTRODUCTION

The heating of streams is receiving growing attention for many reasons some of which are; the chemical reaction velocities and their effect upon the oxygen balance, the dissolved oxygen levels at higher temperatures, fish diseases and parasite activity and aequatic growths. Recent regulations for water standards make accurate temperature forecasting and stream temperature control an important factor in maintaining stream quality within or at the prescribed standards.

Of the factors which cause water in a stream to have a temperature rise we recognize those of natural and man made origin. The investigations discussed in this report deal exclusively with natural causes and particularly with the heat exchange between the terrain and the surface of the stream and the reduction of radiant heat influx because of terrain shading.

When a stream flows through flat terrain and has low banks with low vegetation the contribution of terrain heating may be ignored. However to those streams that flow through deep canyons and between heavily forested banks the effects of longwave radiation heating and shading should be known before we can summarily dismiss such effects in our analysis. This is especially true for streams of minor magnitude which sometimes are completely covered by trees.

PURPOSE AND SCOPE

The Analysis of Stream heating from natural sources has been carried out with considerable success by Duttweiler, Mersinger, Chutchil and Delay-etol. It may therefore appear superfluous to worry about such details as terrain heat contributions. As has been mentioned each stream has its own regimen of terrain and this analysis is only of value when terrain of considerable height and nearness to the stream is under consideration.

In order to determine the effects of terrain radiation, the study problem was divided into three parts. First, the format for data analysis, preferably by a computer. Secondly, a field study to verify the experimental results in a prototype situation, and thirdly an analysis and field study to check the effect of shading by terrain from direct (shortwave) solar radiation.

THE ANALOG TERRAIN MODEL

RADIATION EXCHANGE

The effects of radiation exchange between radiating surfaces in nature may be treated in a manner similar to the radiation exchange in heat transfer of mechanical devices.

In the heat exchange between natural opaque materials a portion of the incident radiation is absorbed, the remainder is reflected. The percent of this portion which is absorbed depends on the nature of the material itself. Some materials are good absorbers; others are better reflectors. Natural materials found along streams such as rocks, soil and vegetation are mainly good absorbers. Any body having a temperature above absolute zero (-273° C) radiates energy. The efficiency of a body to emit radiant energy is its emmisivity. In general good absorbers are also good emitters.

The radiant energy given off by a body is given by the Stefan-Boltzmann equation which states that a body radiates energy directly proportional to the fourth power of its absolute temperature.

$$\text{or } E \sim T^4 \qquad (1)$$

The units are proportioned by σ the proportionality constant. The equation $E = \sigma T^4$ is only valid if a body is a perfect emitter. In nature there are no such emitters and therefore another constant reflecting the particular emmisivity of a material must be included in the equation.

$$Eb = \epsilon \sigma T^4 \qquad (2)$$

In order to determine the efficiency of radiating surfaces and the total emissive power of a surface, consider a hemisphere above a surface dA. (3)

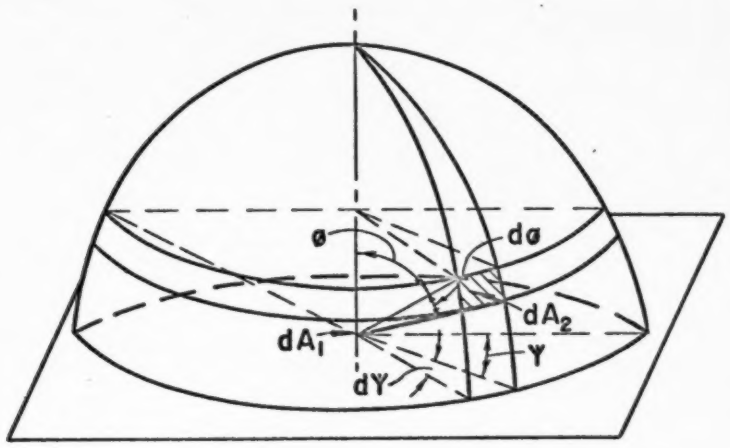

FIG. I
NOMENCLATURE FOR INTENSITY OF RADIATION

This hemisphere receives all radiation beams incident upon it from the element dA. Only directly above it, however is dA seen without distortion.

Viewed from any other position on the hemisphere at a postion Ø from the normal dA, the area only appears to have a size $dA_1 \cos Ø$.

To find the heat emitted by dA_1 and received by dA_2, we use a term called intensity. Intensity is defined as the radiant energy propagated in a particular direction area per unit solid angle and

per unit of area dA_1 as propagated on a plane perpendicular to the direction of propagation. Referring to fig. 1 the intensity is so defined that the rate of radiant heat flow from dA_1 to dA_2 is

$$dq_{1-2} = I \cos \phi \, dA_1 \quad (dA_2/r^2) \tag{3}$$

where $dA_1 \cos \phi$ is effective area as seen from dA_2. By definition dA_2/r^2 is the unit solid angle in the direction of radiation propagation per definition of a solid angle i.e. $d = dA_2/r^2$.

then

$$I = dq_{1-2} \Big/ dA_{1_p} \, d\omega_1 \tag{4}$$

For diffuse surfaces which obey Lambert's cosine law the radiation is constant and does not vary with the emission angle ϕ. To find the total emmissive power of dA_1 we can integrate over the entire hemisphere such that

$$E = \iint_{A_2} I \cos \phi \, \frac{dA_2}{r^2} \tag{5}$$

$d\omega = dA_2/r^2$ may also be written as $\dfrac{(r \sin \phi)(d\Psi)(r d\phi)}{r^2}$

Then

$$E = I \int_0^{2\pi} d\psi \int_0^{\pi/2} \sin \phi \cos \phi \, d\phi.$$

Which integrated gives

$$E = \pi I \tag{6}$$

Thus the total emmersive power E of a surface is π times its intensity.

VIEW FACTORS

Next consider the heat flow not only from dA_1 to dA_2 but also the heat flow from dA_2 to dA_1.

Starting with two surraces dA_1 and dA_2 seperated by a medium which does not absorb radiation appreciable (i.e. air), it is necessary first to determine the fraction of energy leaving surface A_1 which strikes A_2 and then consider the reverse process. The heat flow from dA_1 to dA_2 is

$$dq_{1-2} = I_1 \cos \phi_1 \, dA_1 \, d\omega_{1-2} \qquad (7)$$

where I_1 is the intensity of radiation from dA_1

$dA_1 \cos \phi$ is the projection of area element dA_1 as seen from dA_2

$d\omega_{1-2}$ is the solid angle subtended by receiving area dA_2 with respect to center point of dA_1

$d\omega_{1-2}$ is the projected area of the receiving surface in the direction of the incoming radiation divided by the square of the distance between dA_1 and dA_2.

$$d\omega_{1-2} = \cos \phi_2 \quad \frac{dA_2}{r^2}$$

substituting this equation and $I = \frac{E}{\pi}$ into the expression for dq_{1-2} result in:

$$dq_{1-2} = \frac{Eb_1}{\pi} \quad (\cos \phi_1 \, dA_1)(\cos \phi_2 \frac{dA_2}{r^2})$$

The total radiation from dA_2 striking dA_1 is by analogy

$$dq_{2-1} = \frac{Eb_2}{\pi} \quad (\cos \phi_2 \, dA_2)(\cos \phi_1 \frac{dA_1}{r^2})$$

Then the net rate of heat flow between these elements is

$$dq_{2\rightleftharpoons 1} = (Eb_1 - Eb_2) \frac{\cos \phi_1 \cos \phi_2 \, dA_1 \, dA_2}{r^2}$$

The net rate of the heat flow between the entire surfaces is the integration of this expresstion or

$$dq_{1\rightleftharpoons 2} = (Eb_1 - Eb_2) \int_{A_1} \int_{A_2} \frac{\cos\phi_1 \cos\phi_2 \, dA_1 \, dA_2}{r^2} \qquad (8)$$

The double integrat is written in shorthand form as

$$A_1 F_{1-2} \text{ or } A_2 F_{2-1} \qquad (9)$$

where F_{1-2} and F_{2-1} are called the shape or view factors evaluated on the basis of A_1 and A_2 respectively.

Physically F_{1-2} represents the fraction of the total radiant energy leaving A_1 which is intercepted by A_2 and F_{2-1} is the fraction of energy reaching A_1 from A_2, thus: $A_1 F_{1-2} = A_2 F_{2-1}$.
The heat flow expression is then

$$dq_{1\rightleftharpoons 2} = (Eb_1 - Eb_2) F_{1-2} A_1 = (Eb_1 - Eb_2) F_{2-1} A_2 \qquad (10)$$

The problem lies in obtaining the view factor which except for any except the most simple geometrical forms is very complex. It is therefore necessary for application purposes to simplify the procedure of obtaining the view factor.

In fig. 1, dA_1 has a view factor of unity because all emitted radiation is intercepted by the hemisphere above it. Let dA be a water surface and the hemisphere is the air above it. A terrain obstruction blocking part of this hemisphere will change the atmosphere view factor. The reduction in the hemisphere view factor is equal to the view factor of the terrain causing this reduction.

A semi-graphical solution for determining the view factor is presented here which produces acceptable results.

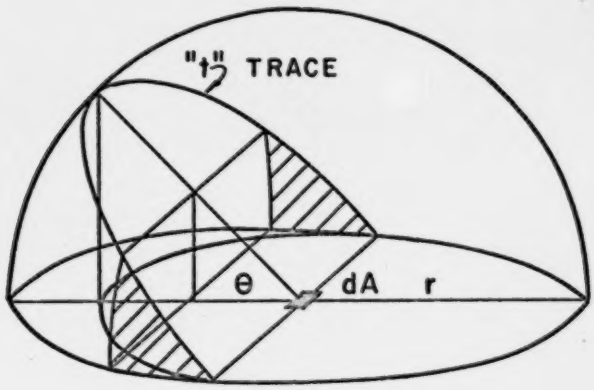

FIG. 2
VIEW FACTOR REDUCTION BY OBSTRUCTION

In fig. 2 part of the hemisphere is blocked by a canyon wall or trees along the river edge. A plane passing through the top of the trees and dA has an inclination of θ with the horizontal plane. This plane cuts an imaginary hemisphere as trace "t". If this trace is projected on the horizontal circle of radius r, then the portion falling outside the projected trace is the reduction in the hemisphere view factor of 1, this is shown in the next paragraph.

From texts on heat transfer the view factor relationship for a plane of infinite extent having an angle θ with the horizontal plane and dA is obtained. This relationship is $F_{dA_1-A_2} = \frac{1}{2}(1 + \cos\theta)$ if θ is larger than 90° the cos value becomes negative. Thus for a 45° slope away from dA_1 of a θ angle of 135° as in fig. 2.

$$F_{dA_1-A_2} = \frac{1}{2}(1 - \cos 45^\circ)$$

$$" = \frac{1}{2}(1 - 0.707)$$

$$" = \frac{1}{2}(0.293)$$

$$F_{dA_1\ A_2} = 0.147$$

This is compared with the ratio reduction of the area of an ellipse with that of a circle. fig. 3

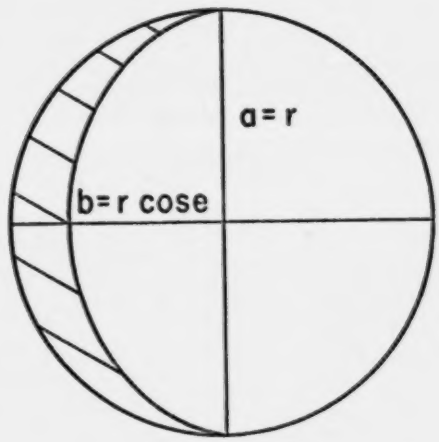

FIG. 3
GRAPHICAL PRESENTATION OF VIEW FACTOR

Area reduction in percent $= \frac{A_{circle} - A_{ellipse}}{A_{circle}}$

$$= \frac{\pi r^2 - \pi r^2 \cos\theta}{r^2}$$

$$= 1 - \cos\theta$$

If this applies to only one side then

Percent area reduction = $\frac{1}{2}(1 - \cos\theta)$

which is the same as the view factor for an infinite plane at angle θ with dA. Where θ is defined as in fig 2.

This is the view factor of the water surface dA emitting to the terrain (one side only.)

If the terrain were symmetrical then $F_{water\text{ - }terrain} = F_{w-t} = (1-\cos\theta)$. The atmospheric view factor is the $F_{water\text{- }air} = F_{w-a} = 1 - \frac{1}{2}(1-\cos\theta)$. $F_{w-a} = \frac{1}{2}(1+\cos\theta)$ for one side being obstructed and $\cos\theta$ for a symmetrical problem.

A slight discrepancy is introduced in this treatment by the fact that the shaded areas in fig. 2 are included as part of the atmosphere view factor reduction. The effect is minor since the projection does not materially alter the solution.

Since $A_w F_{w-a} = A_a F_{a-w}$ and

$A_w F_{w-t} = A_t F_{t-w}$

we will assume that A_w is a unit area (i.e. ISF).

Then $dq_{w \rightleftharpoons t} = (E_w - E_t) A_w F_{w-t} = (E_w - E_t) A_t F_{t-w}$

$dq_{w \rightleftharpoons t} = (E_w - E_t)(1\ SF)\ F_{w-t}$

and $dq_{w-a} = (E_w - E_a)(1\ SF)\ F_{w-a}$

In considerations not involving terrain radiation the longwave radiation exchange is handled with the equation

$$E_{b_w} = 0.97 \sqrt{} (T_w^4 - \beta T_a^4) \qquad (11)$$

where E_{b_w} = Net longwave radiation exchange between air at a temperature T_a and water at T_w.

0.97 is included in the reflectivity of the water surface for incoming atmospheric radiation and is also the emmisivity of the water surface itself.

β is a factor which represents the integrated temperature value at which the atmospheric mass of particles radiates. This value which varies with cloud cover and vapor pressure may on clear days be taken as ranging between 0.75-0.85 and for this problem will be taken as 0.80.

A schemetic diagram of radiation exchange as represented between a surface of water of infinite size and air is shown in fig. 4.

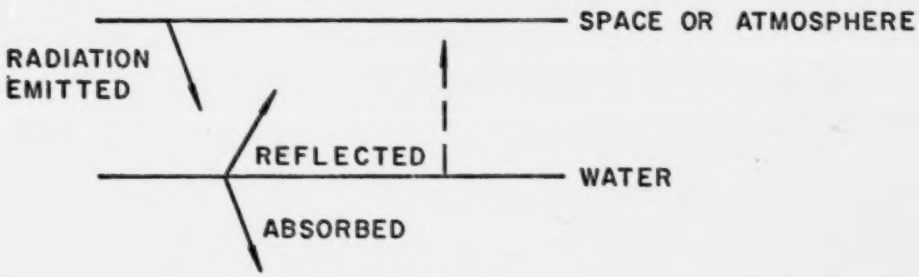

FIG. 4
RADIATION EXCHANGE BETWEEN INFINITE SURFACES

When the problem of terrain radiation is included , the radiation exchange is approximately as is shown in fig. 5.

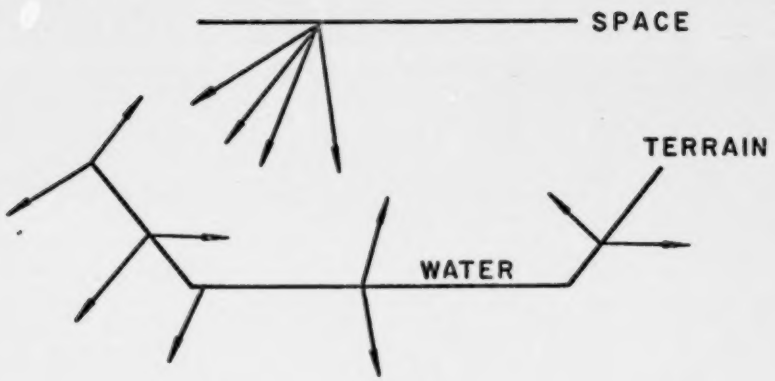

FIG. 5
RADIATION EXCHANGE BETWEEN FINITE SURFACES

In this diagram radiation from space is shown as being absorbed and reflected by the terrain. The terrain then radiates back to the atmosphere and to the water surface and other terrain.

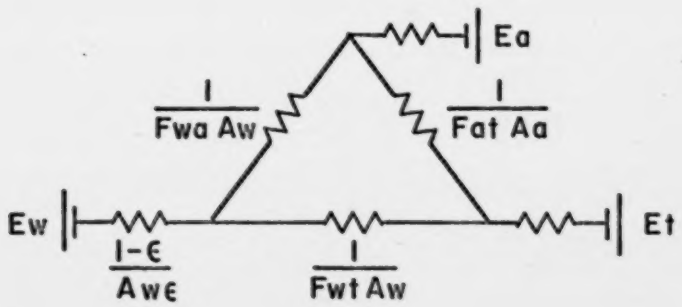

FIG. 6
ANOLOG CIRCUIT REPRESENTING RADIATION EXCHANGE BETWEEN FINITE SURFACES

ANALOG CIRCUITS

The solution to the model is found by the use of an analog computer model which in turn may be represented by a series of equations which when solved simultaneously gives the heat flow from one surface to another.

In the bridge circuit shown in fig. 6 "t" is used to describe terrain, "w" identifies water and "a" is used for air. The temperatures of each of these surfaces determines their effective emissive potential as determined by the Stephan-Boltzmann equation $E = \epsilon \sigma T^4$ and is represented by a potential source which is grounded. The emissivities are obtained by resistors in the legs to the bridge circuit and the view factors which determine the heat flow are obtained by resistors in the legs of the bridge circuit.

The resistance of the emissivity resistors is found from (1)

$$R = \frac{1 - \epsilon}{A_w \epsilon} \qquad \text{Units of } R = 1/\text{S.F.}$$

R = Resistance

ϵ = Emissivity

A_w = Area of water radiating to surroundings

The value of the resistors for atmosphere and terrain emissivity approach zero because A_a and A_t are so very large compared to A_w which is one square foot that the function for the resistor goes to zero.

The β factor is sometimes considered as an emissivity factor but it cannot be considered as such. It is rather the integrated value of all particles radiating. The emissivity of these particles in the air

is presumed to be 1.0 or near to it, but since they are dispersed in the atmosphere at different temperatures their sum total radiation is less that that of the air temperature observed near the ground. The molecules of O_2, N_2, etc. do not absorb or emit radiant energy. The resistors in the legs of the circuit are computed using the function $R = \frac{1}{A_w F_{wt}} = \frac{1}{A_t F_{tw}}$. This represents the resistor between water and terrain. The resistor between air and terrain may again be reduced to zero because either A_t or A_a are large compared to A_w.

The bridge circuit then takes on the simplified form shown in fig. 7.

Three loop equations may be written for this circuit where I (current) is the heat flow between the potentials in such a way that $E = IR$ corresponds to $dq_{wa} = \Delta E \; A_w \; F_{wa}$

$$\text{or} \quad \Delta E = \frac{dq_{wa}}{A_w F_{wa}} = dq_{1-2} \; \frac{1}{A_w F_{wa}}$$

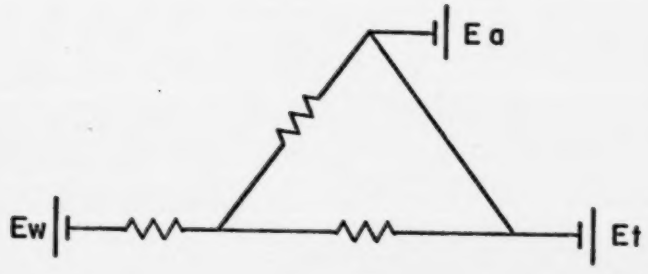

FIG.7
SIMPLIFIED ANALOG CIRCUIT OF RADIATION EXCHANGE BETWEEN INFINITE SURFACES

EXAMPLES AND SOLUTION OF ANALOG MODEL

An example solution is given here. Starting with a terrain source of trees along a river bank height 100 feet and the stream is 100 feet wide, tree temperature 86° F, air temperature 90° F, and water temperature 65° F. The view factor for a SF of water in the middle of the stream is

$$F_{w-t} = \frac{1}{2} (1-\cos \theta).$$

$$= \arctan \frac{\text{tree height}}{\frac{1}{2} \text{ river width}}$$

$$F_{wt} = \frac{1}{2} (1-\cos \arctan \frac{100}{50})$$

$$= \frac{1}{2} (1-\cos 62.5^{\circ})$$

$$= \frac{1}{2} (1- .422)$$

$$= \frac{1}{2} (0.578)$$

$$= 0.289 = 0.29$$

$$F_{wa} = 1 - 0.29 = 0.71$$

Then

$$R_w = R_1 = \frac{1-\epsilon}{A_w \epsilon} = \frac{1.0 - 0.97}{1\ (0.97)} = 0.03 \ \frac{1}{SF}$$

$$R_{wa} = R_2 = \frac{1}{A_w F_{wa}} = \frac{1}{1\ (0.71)} = 1.41 \ \frac{1}{SF}$$

$$R_{wt} = R_3 = \frac{1}{A_w F_{wt}} = \frac{1}{1\ (0.29)} = 3.45 \ \frac{1}{SF}$$

The potentials are taken from table 1 which lists the values of the longwave radiation of water at varying temperatures. The emissivity

factor of 0.97 is included.

TABLE 1
RADIATION OF ATMOSPHERE OR WATER TO ENVIRONMENT
AT ABSOLUTE ZERO,[a]
(in Btu per square foot per hour)

Temperature, in °F	Temperature, in °F									
	0	1	2	3	4	5	6	7	8	9
0	74.2	74.8	75.5	76.1	76.8	77.7	78.7	79.3	79.6	80.2
10	80.8	81.5	82.2	82.9	83.6	84.3	85.1	85.8	86.5	87.2
20	88.0	88.6	89.4	90.2	90.9	91.7	92.4	93.2	94.0	94.7
30	95.5	96.3	97.1	97.9	98.7	99.5	100.3	101.1	101.9	102.7
40	103.6	104.4	105.2	106.1	106.9	107.8	108.6	109.5	110.4	111.2
50	112.2	113.0	113.9	114.8	115.7	116.6	117.5	118.4	118.3	120.3
60	121.2	122.1	123.1	124.0	125.0	125.9	126.9	127.8	127.8	129.8
70	130.8	131.8	132.8	133.8	134.8	135.8	136.8	137.8	138.9	139.9
80	140.9	142.0	143.0	144.1	145.2	146.2	147.3	148.4	149.5	150.6
90	151.7	152.8	153.9	155.0	156.2	157.3	158.4	159.6	160.7	161.9
100	163.0	164.2	165.4	166.6	167.7	168.9	170.1	171.3	172.6	173.8
110	175.0	176.2	177.5	178.7	180.0	181.2	182.5	183.8	185.0	186.3

[a]Includes effect of emissivity for water and reflectivity for atmospheric radiation.

This provides $E_w = 126$ BTU/SF/HR

$$E_a = \frac{1}{0.97} (0.80)(15.7) = 125.1 \text{ BTU/SF/HR}$$

$$E_t = \frac{1}{0.97} (147.3) = 151.9 \text{ BTU/SF/HR}$$

The table is prepared for the effective radiation of water including the factor 0.97. This factor must therefore be removed from the radiative potentials of other materials. The values shown are for the effective radiation temperature of the substances involved and this is generally a few degrees lower than the observed values depending on their emissivity constants.

Solving this for the circuit shown in fig. 7 with the addition of a real small resistor in the leg between air and terrain to indicate

that there is heat flow between terrain and air, the following equations develop providing I_1 is in the leg going to E_w. I_2 is away from the junction at E_w going to E_a and I_3 is going to the junction at E_w. I_4 may be considered in the side between E_a and E_t but will drop out of the solution.

The development of an analog circuit for atmosphere and two terrain sources of different temperatures may be similarly developed.

RESULTS:

$$I_1 = I_3 - I_2$$

$$+ I_2R_2 + I_4R_4 + I_3R_3 = 0$$

$$E_w + R_1I_1 - R_2I_2 - E_a = 0$$

$$E_w + R_1I_1 + R_3I_3 - E_t = 0$$

In matrix form this is:

$$\begin{vmatrix} 1 & 1 & -1 & 0 \\ 0 & R_2 & R_3 & R_4 \\ R_1 & -R_2 & 0 & 0 \\ R_1 & 0 & R_3 & 0 \end{vmatrix} \begin{vmatrix} I_1 \\ I_2 \\ I_3 \\ I_4 \end{vmatrix} = \begin{vmatrix} 0 \\ 0 \\ E_a-E_w \\ E_t-E_w \end{vmatrix}$$

from which I matrix may be found but since only I_1 is of interest, only I_1 is shown:

$$I_1 = \frac{+R_2 (E_t-E_w) + R_3 (E_a-E_w)}{R_1R_2 + R_2R_3 + R_1R_3}$$

With an input of

$$R_1 = 0.03 = \frac{1-\epsilon}{A_w\epsilon} = \frac{1 - 0.97}{1 (0.97)}$$

$$R_2 = 1.41 = \frac{1}{A_w F_{wa}} = \frac{1}{1 (0.91)}$$

$$R_3 = 3.44 = \frac{1}{A_w F_{wt}} = \frac{1}{1\ (0.29)}$$

and

$E_w = 126$ BTU/SF/HR

$E_a = 125.1$ "

$E_t = 151.9$ "

and for the heat flow

$I_1 = 6.7$ BTU/SF/HR

$I_2 = .8$ "

$I_3 = 7.5$ "

OTHER METHODS FOR VIEWFACTOR EVALUATION

Another way of calculating view factors may be found as follows: Since most canyons and trees along streams form a plane which can be generated by a line parallel to the plane of dA_1, the following relationship may be derived from fig. 8.

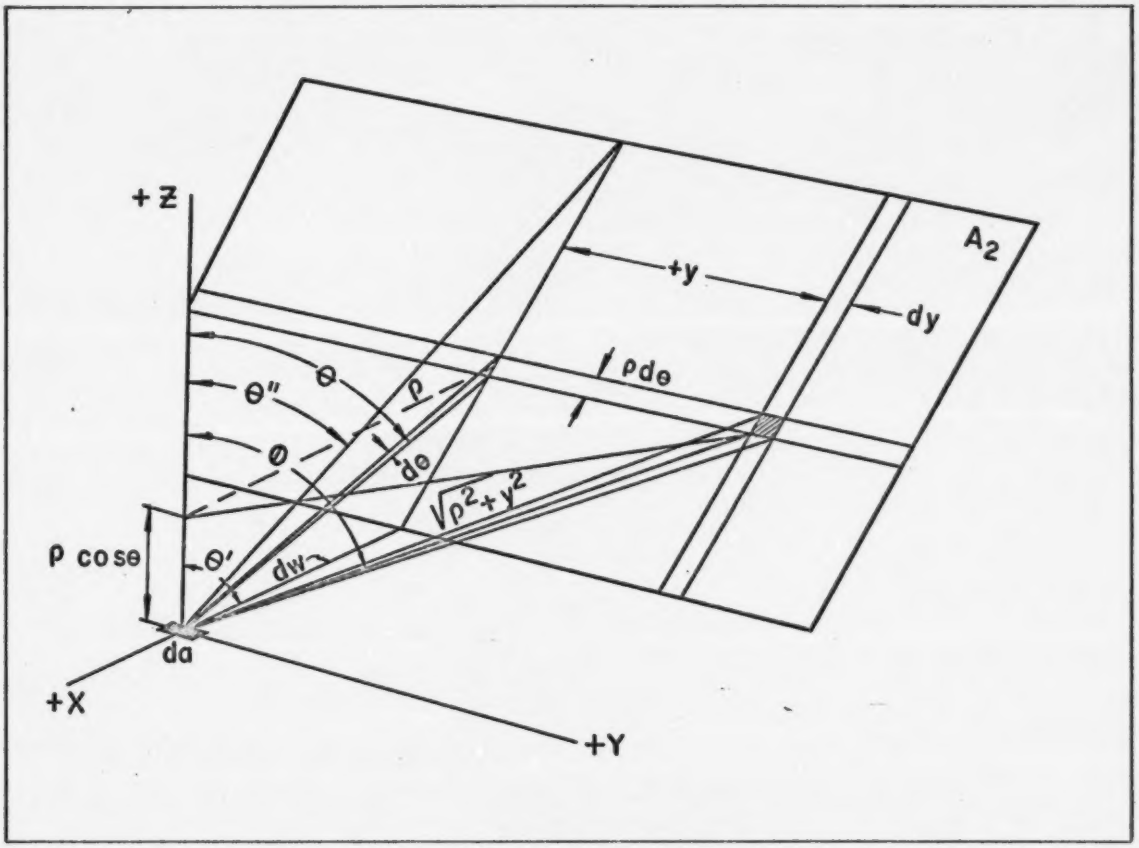

FIG. 8
VIEW FACTOR ANALYSIS OF PARALLEL PLANE

$$\cos \phi = \frac{\cos \theta}{(\rho^2 + y^2)^{1/2}} \tag{12}$$

$$d\omega_1 = \frac{d\theta\, dy}{\left[(\rho^2+y^2)^{1/2}\right]^2} \left(\frac{\rho}{(\rho^2+y^2)^{1/2}}\right) \tag{13}$$

where the last element of the equation introduces the variability along y of dA_2.

The introduction of cos ϕ in to $d\omega_1$ covers the variability of dA_2 with respect to a varying ϕ up and down due to different y positions.

Then the general expression for $d\omega$ is

$$d\omega_1 \cos \phi = \rho^3 \frac{\cos \theta \, d\theta \, dy}{(\rho^2 + y^2)^2} \qquad (14)$$

integrating for $d\theta$ between θ' (bottom) and θ'' (top) and for y between $-\infty$ and $+\infty$ there is obtained for the heat flow between dA_1 and A_2

$$q_{1 \rightleftharpoons 2} = \sigma (T_1^4 - T_2^4) \, dA_1 \, \frac{1}{\pi} \int_{-\infty}^{+\infty} \int_{\theta''}^{\theta'} \rho^3 \frac{\cos\theta \, d\theta \, dy}{(\rho^2 + y^2)^2} \qquad (15)$$

$$q_{1 \rightleftharpoons 2} = \sigma (T_1^4 - T_2^4) \, dA_1 \quad \frac{\sin\theta' - \sin\theta''}{2}$$

or $$q_{1 \rightleftharpoons 2} = \sigma (Eb_1 - Eb_2) \, dA_1 \quad F_{1-2}$$

where $$F_{1-2} = \frac{\sin\theta' - \sin\theta''}{2} \qquad (16)$$

The integration of expression (15) is shown in Appendix "A".

In the example used with method 1 a view factor for the forest on one side of the stream of $F_t = 0.29$ was obtained.

The angle from the stream surface at dA_1 in the middle of the stream to the top of the trees was 62.5°. This for method 2 the $\theta'' = 90 - 62.5$ and $\theta' = 90^\circ$.

Thus
$$F_w t = \sin 90^\circ - \sin 62.5^\circ$$
$$= \frac{1 - 0.46}{2}$$
$$= 0.27$$

This value agrees closely with that obtained by method 1.

PROTOTYPE FIELD STUDIES OF TERRAIN RADIATION

Prototype field studies have been conducted on several sites along Oregon Streams to determine terrain temperatures of rocks and trees.

The basic instrumentation for field studies was a Barnes IT-3 Infra-Red thermometer which operates on 110 A.C. thus requiring a portable generator for power source. The IT-3 with a 3^{o} optical window views the heat energy emission in the 8 - 13μ range where the atmosphere is transparent. The sensing head of this instrument was mounted on a specially made horizontal axis fitted to the standards of regular transit, fig. 9.

fig. 9

A 10-turn rotating potentiometer was attached to the outside frame and was activated by a rubber edged wheel riding on the

horizontal circle as it moved through a 360° turn. The output from the IT-3 and the potentiometer were then fed to the Y and X terminals of Moseley 135A, X-Y recorders. The trace thus obtained forms an integrated temperature trace of the terrain viewed by the optical system of the sensing head. Elevating the line of sight of the sensing head by means of the transit vertical circle permits the evaluation of the terrain at the different levels as viewed by the system.

Such traces typical of the data obtained shown in fig's 10 and 11 for elevation angles of 0 and 20.

The analysis for data reduction takes the graph from the X-Y recorder and averages the terrain temperature for sections of the terrain between different Azimuths. Gaps in the curve indicate that the optical system views the transparent sky. The Azimuth of the downstream direction of the stream is taken at zero, the sky gaps appearing in line with 0° and 180° define then in general the two sides of the terrain. The angle of this terrain to incoming solar radiation determines its surface temperature to a great extent. The view factor of terrain surrounding a spot on a stream may be found from

$$F_{w-t} = \sin^2 (\arctan \theta) \qquad (17)$$

where F is the view factor of the water surface element dA_1

θ is the elevation angle of the terrain as viewed from dA_1

It is readily evident that high and lows in this circular sky opening make the horizon outline ragged. The use of the IT-3 with the XY recorder allows a trace to be obtained where the average terrain

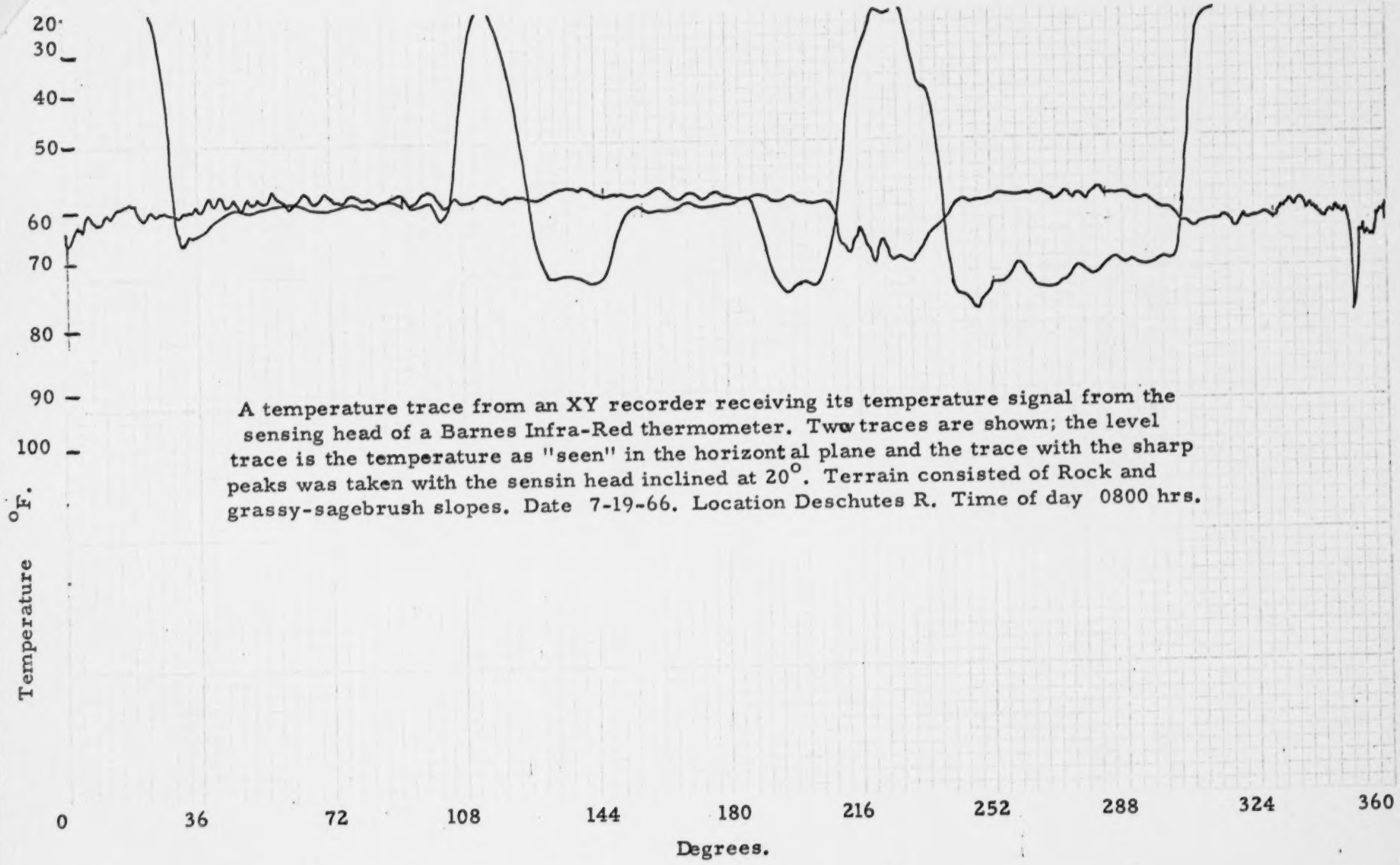

A temperature trace from an XY recorder receiving its temperature signal from the sensing head of a Barnes Infra-Red thermometer. Two traces are shown; the level trace is the temperature as "seen" in the horizontal plane and the trace with the sharp peaks was taken with the sensin head inclined at 20°. Terrain consisted of Rock and grassy-sagebrush slopes. Date 7-19-66. Location Deschutes R. Time of day 0800 hrs.

Fig. 10

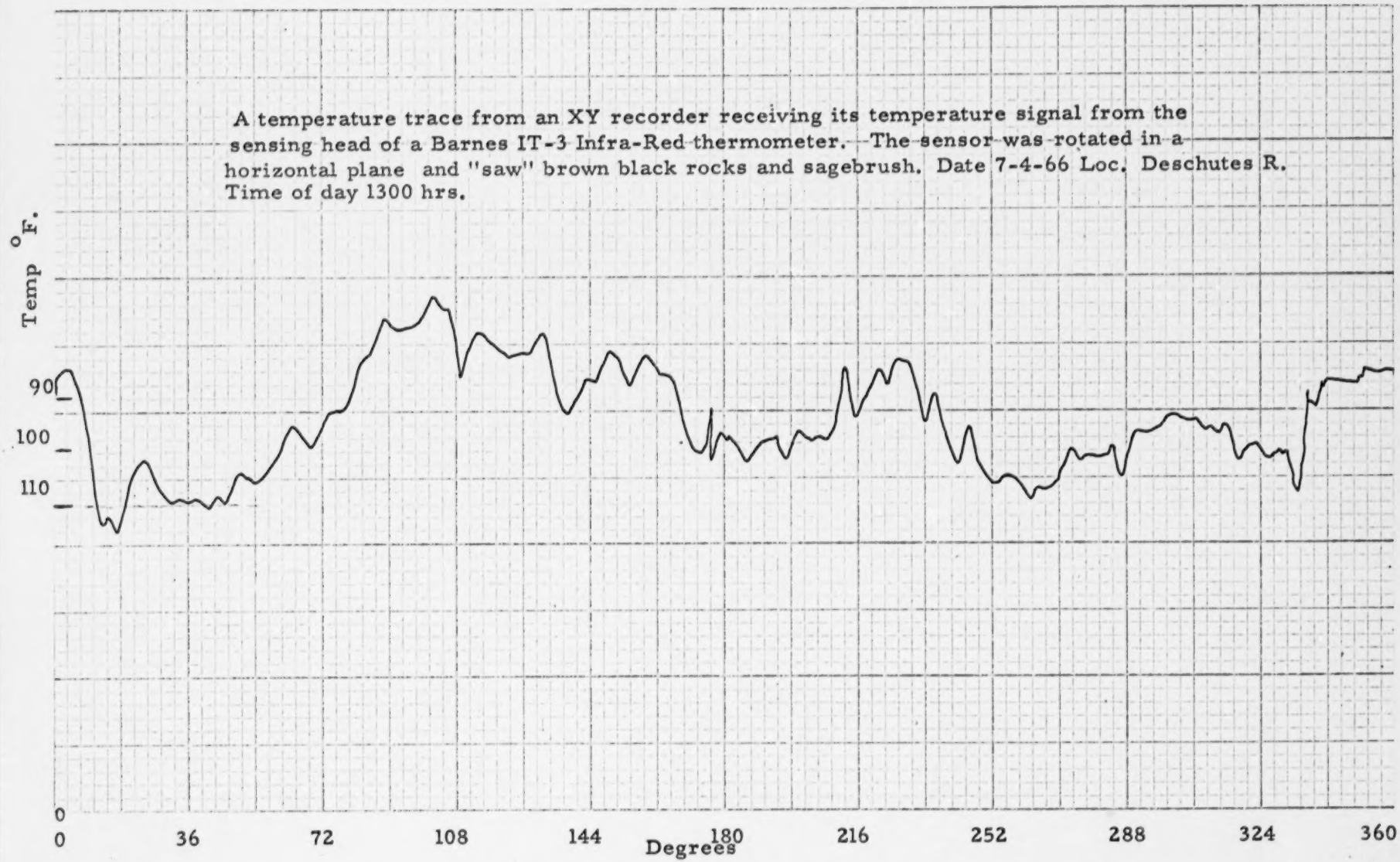
A temperature trace from an XY recorder receiving its temperature signal from the sensing head of a Barnes IT-3 Infra-Red thermometer. The sensor was rotated in a horizontal plane and "saw" brown black rocks and sagebrush. Date 7-4-66 Loc. Deschutes R. Time of day 1300 hrs.
Temp °F.
90
100
110
0
0
36
72
108
144
180
216
252
288
324
360
Degrees

Fig. 11

elevation angle can be estimated from the graphs obtained and from visual observation while viewing the terrain on the site.

Thus the view factor may be calculated from the sum of a series of composites each of which is a fraction $F_n = \frac{n}{360} \sin^2 (\text{arc tan } Z/X)$ where n is the number of degrees found to have a specified temperature on an horizon trace. $F = \sum F_n$.

If the terrain temperature is uniform then the view factor so found as above or by means of previously outlined methods is used to calculate the heat flow using the analog circuit.

For terrain of several temperatures a more complex analog circuit must be used with the view factors calculated on the basis of the horizon segment occupied by this terrain or the radiation intensities must be weighted on the basis of their respective view factors and then averaged. The resulting radiation intensity is then employed with the composite view factor for network analysis.

For terrain elevation angles of less than 10^o the effect of terrain radiation will be very slight but for angles of 20^o or greater especially when these angles surround the stream the view factor becomes appreciable, amounting to approximately 0.10 - 0.12 and then, depending on the surrounding terrain temperatures, become a factor of importance in stream temperature analysis. The view factor for site 1 on the Deschutes River is calculated in table 2 using the horizon trace shown in fig. 12.

In most cases the perpendicular elevation angle as discussed in the earlier part of the report will give the simplest solution for the view factor. Rogue River site was essentially a wedge and thus the

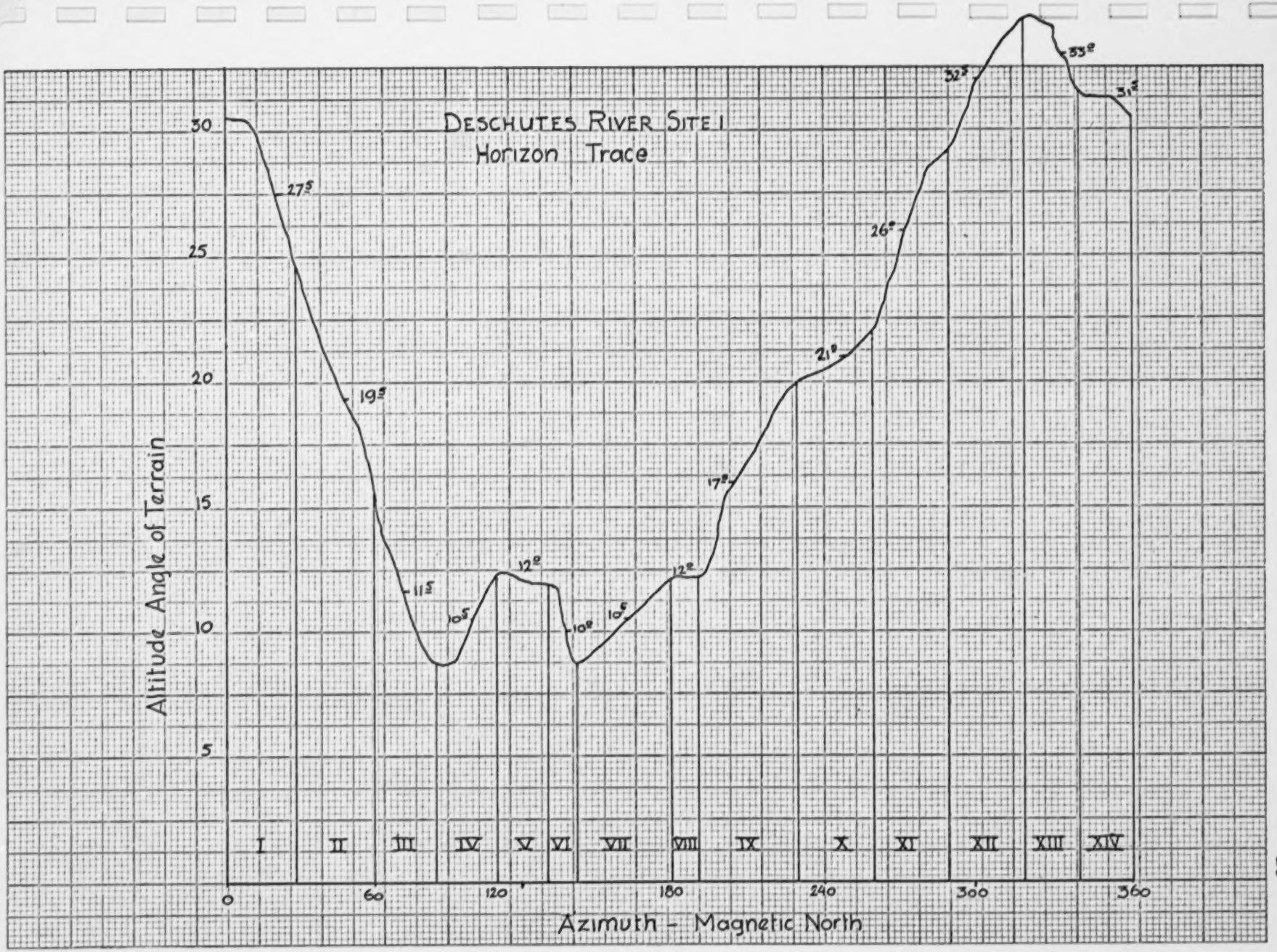
DESCHUTES RIVER SITE I
Horizon Trace
Altitude Angle of Terrain
30
25
20
15
10
5
27°
19°
11°
10°
12°
10°
10°
12°
17°
21°
26°
32°
33°
31°
I
II
III
IV
V
VI
VII
VIII
IX
X
XI
XII
XIII
XIV
0
60
120
180
240
300
360
Azimuth - Magnetic North

fig. 13

slope angles were used to find the view factor, Side slopes were 30° and 42.5°, which gives a combined view factor of $F_{w-t} = 0.213$.

F_I	=	1/12	$\sin^2 (27.5^{\circ})$	=	.0176
II	=	1/12	$\sin^2 (24.5^{\circ})$	=	.0139
III	=	25/360	$\sin^2 (11.5^{\circ})$	=	.0028
IV	=	25/360	$\sin^2 (10.5^{\circ})$	=	.0022
V	=	1/18	$\sin^2 (12.0^{\circ})$	=	.0024
VI	=	1/36	$\sin^2 (10.0^{\circ})$	=	.0008
VII	=	1/9	$\sin^2 (10.5^{\circ})$	=	.0037
VIII	=	1/36	$\sin^2 (12.5^{\circ})$	=	.0013
IX	=	1/9	$\sin^2 (17.0^{\circ})$	=	.0093
X	=	1/12	$\sin^2 (21.5^{\circ})$	=	.0112
XI	=	1/12	$\sin^2 (26.0^{\circ})$	=	.0161
XII	=	1/12	$\sin^2 (32.5^{\circ})$	=	.0239
XIII	=	1/18	$\sin^2 (33.0^{\circ})$	=	.0167
XIV	=	1/18	$\sin^2 (31.5^{\circ})$	=	.0150
			$F = \Sigma F_n$	=	0.1369
				$\simeq$	0.137
				$\simeq$	0.14

View Factor Calculations for Deschutes Site 1

Table 2

STUDY SITES

Terrain temperature data was obtained for sites along the Rogue River in Southern Oregon and the Deschutes River in Central Oregon. See fig's. 13 and 14.

The Rogue River sites are located along the last 50 miles of the Rogue River in the area where the stream flows through the extension of the Coast Range. Here the canyons or river valleys are deeply incised and mountains rise to 2000-3000 ft. In some areas the stream cuts almost through vertical walled canyons. Most of the slopes are heavily wooded from the floodstage edge to the top of the mountains. Heavy winter flows keep the lower 20 ft. of the banks scoured clean of vegetation. During midsummer this area becomes very dry and hot. In the middle of the day only vertical air currents are noted changing to late afternoon breezes.

The Deschutes sites are in a different part of the state and are in desert terrain. Only sagebrush and grass clothe the slopes alternating with basaltic lava flows which in many of the outer bends of the river present near vertical walls. The valley of the Deschutes is much wider than the Rogue but the mountains still go up 2000-2500 ft. to the high plateau country. This area is extremely dry and the humidity falls to 15% very easily. This stream flows in a general S to N direction while the Rogue River flows generally from E to W. However site 2 on the Rogue was located along a S-N section. Different in location though the sites along the respective streams were with respect to the compass, it did not affect the maximum temperatures reached at the sites considering daily variations were taken into account.

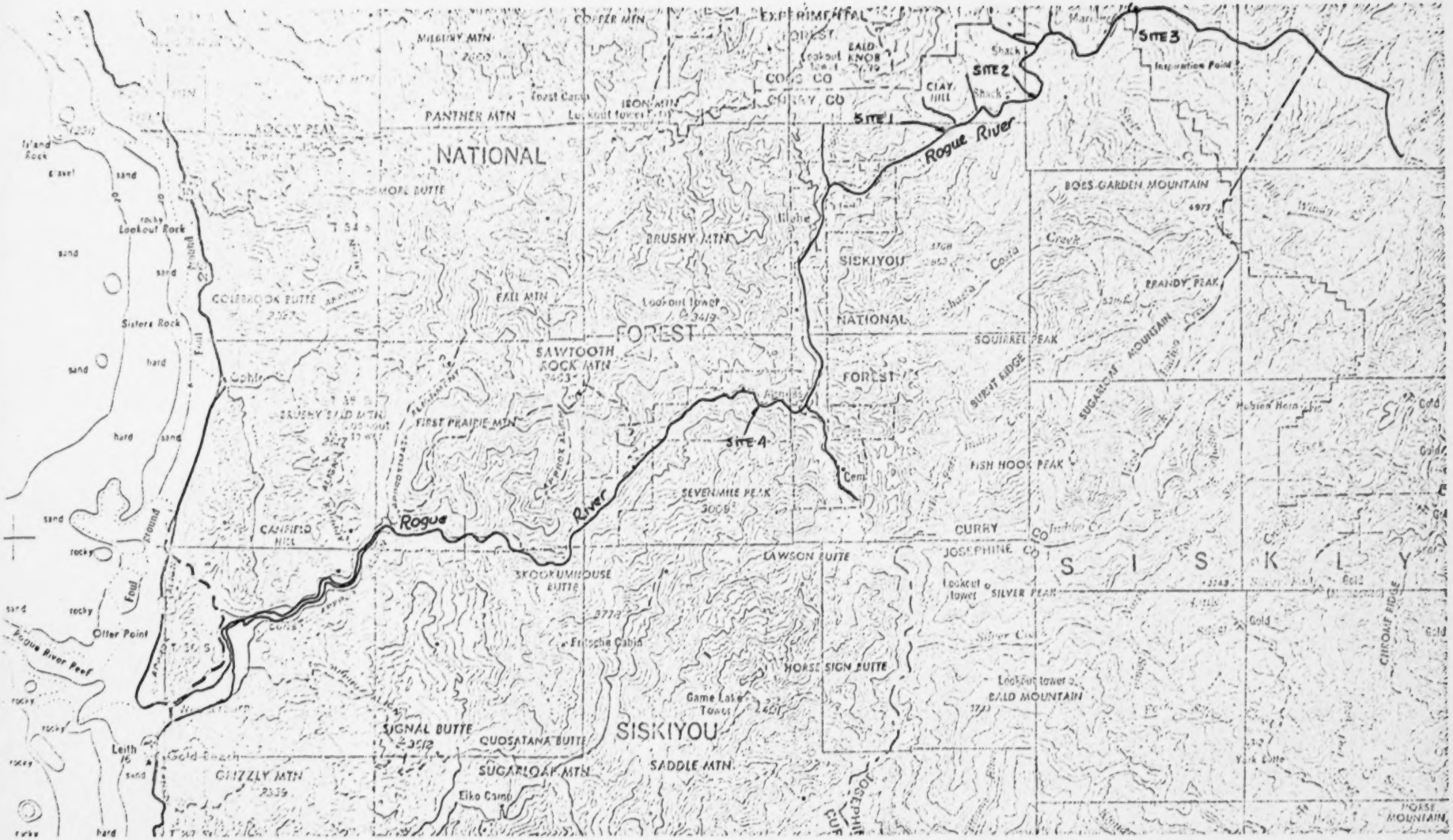
SITE 1
SITE 2
SITE 3
SITE 4
Rogue River
Rogue River
NATIONAL
FOREST
SISKIYOU
NATIONAL
FOREST
SISKIYOU
PANTHER MTN
BRUSHY MTN
FALL MTN
SAWTOOTH ROCK MTN
FIRST PRAIRIE MTN
SEVENMILE PEAK
LAWSON BUTTE
SKOOKUMHOUSE BUTTE
HORSE SIGN BUTTE
SIGNAL BUTTE
QUOSATANA BUTTE
SUGARLOAF MTN
SADDLE MTN
GRIZZLY MTN
BALD MOUNTAIN
SILVER PEAR
FISH HOOK PEAK
SQUIRREL PEAK
BRANDY PEAK
BOES GARDEN MOUNTAIN
SUGARLOAF MOUNTAIN
SUMMIT RIDGE
CHIMNEY ROCK
CAMFIELD HILL
CLAY HILL
BALD KNOB
IRON MTN
MISERY MTN
ROCKY PEAK
Lookout Rock
Sisters Rock
COLEBROOK BUTTE
Otter Point
Rogue River Reef
Leith
Elko Camp
Game Lake Tower
Lookout tower
Lookout tower
Lookout tower
Cabin
Cabin
Cabin

Map of Deschutes River Area

Fig. 14

Typical terrain for sites along these streams is shown in fig's. 15 through 20.

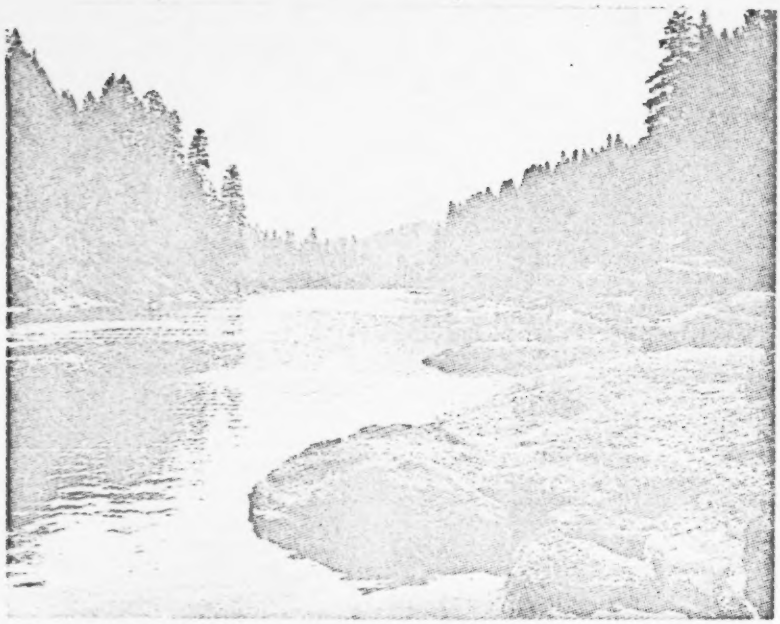

Typical Terrain Along Rogue River -- Site #1.

F_{wt} = .133 (ave. terrain slope 30°)

Fig. 15

Fig. 16

fig. 17

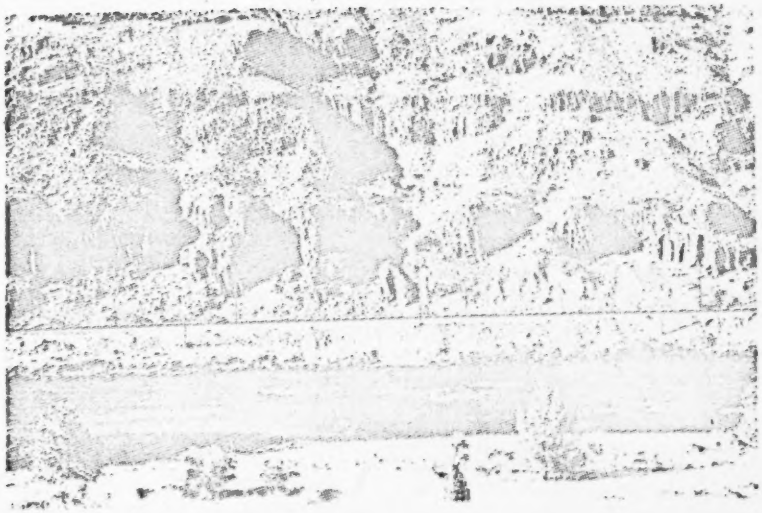

fig. 18

fig. 17

fig. 18

fig. 19

fig. 20

4 sites along each stream were examined and a typical temperature distribution for each stream is shown in tables 3 and 4.

Rogue River

Terrain, Air and Water Temperatures in °F for a clear day

Time	Rocks	Trees	Sand or Gravel	Water (Stream)	Air
0630	57	57	57	66	55
0903	84 Sun 62 Shade	62		65	70
1112	101 Sun 74 Shade	74	92	70	82
1315	104 Sun 75 Shade	80	113	72	87
1530	97 Sun	86	116	72	93
1755	102 Sun 80 Shade	85	115	73	95
1935	80	80	93 Sun 88 Shade	74	84

Table 3

Deschutes River

Terrain, Air and Water Temperatures in °F for a clear day

Time	Rocks	Grass and Sagebrush	Water	Air
0900	78-85 Sun 62 Shade	70	60	74
1100	91 Sun 76 Shade	76	62	78
1315	92.5 Grass slope exposed 107 Sun	86	64	86
1530	90 100 Grassy slope	86	63	81
2020	82	82	61	65
2315	76-79	80	59	61
0530	70-71	71	59	56
0730	71 Sun 68 Shade	68	59	59
1015	95-100 Sun 82 Shade	84	62	76

Table 4

Although only one set is shown for each site, the thermograph and IT-3 records for each type of terrain are very repetitive for each of the sites.

The check on the amount of terrain radiation received by the stream was executed with the same equipment as that used for the laboratory model.

The Kipp Solarimeter was used to obtain the shortwave radiation and a Tanner Economical Net Radiometer, which will be referred to as ENR, for long and short wave radiation determinations from atmosphere, terrain and water. This radiometer was developed by Swan, Federer, and Tanner (7). In addition, thermistors were employed for dry, wet bulb, and stream temperatures.

The Kipp Solarimeter which has a very high precision for measurement of solar radiation (1% error) was used as the primary measurement instrument. The ENR was calibrated for operating characteristics using the Solarimeter. In fig. 21 the correlation between the ENR and the Solarimeter is shown.

DISCUSSION

For discussion purposes the analysis of two sites are shown in this report. The first site is site number 1 on the Rogue River and site number 2 is Deschutes River site number 1 as shown on the maps in fig's. 13, 14 and on photographs in figs 15, 19 and 18, 19 respectively. In fig. 22, three types of curves are presented. One is the ENR longwave length energy flux, two others display the long-wave heat exchange between water atmosphere and terrain using

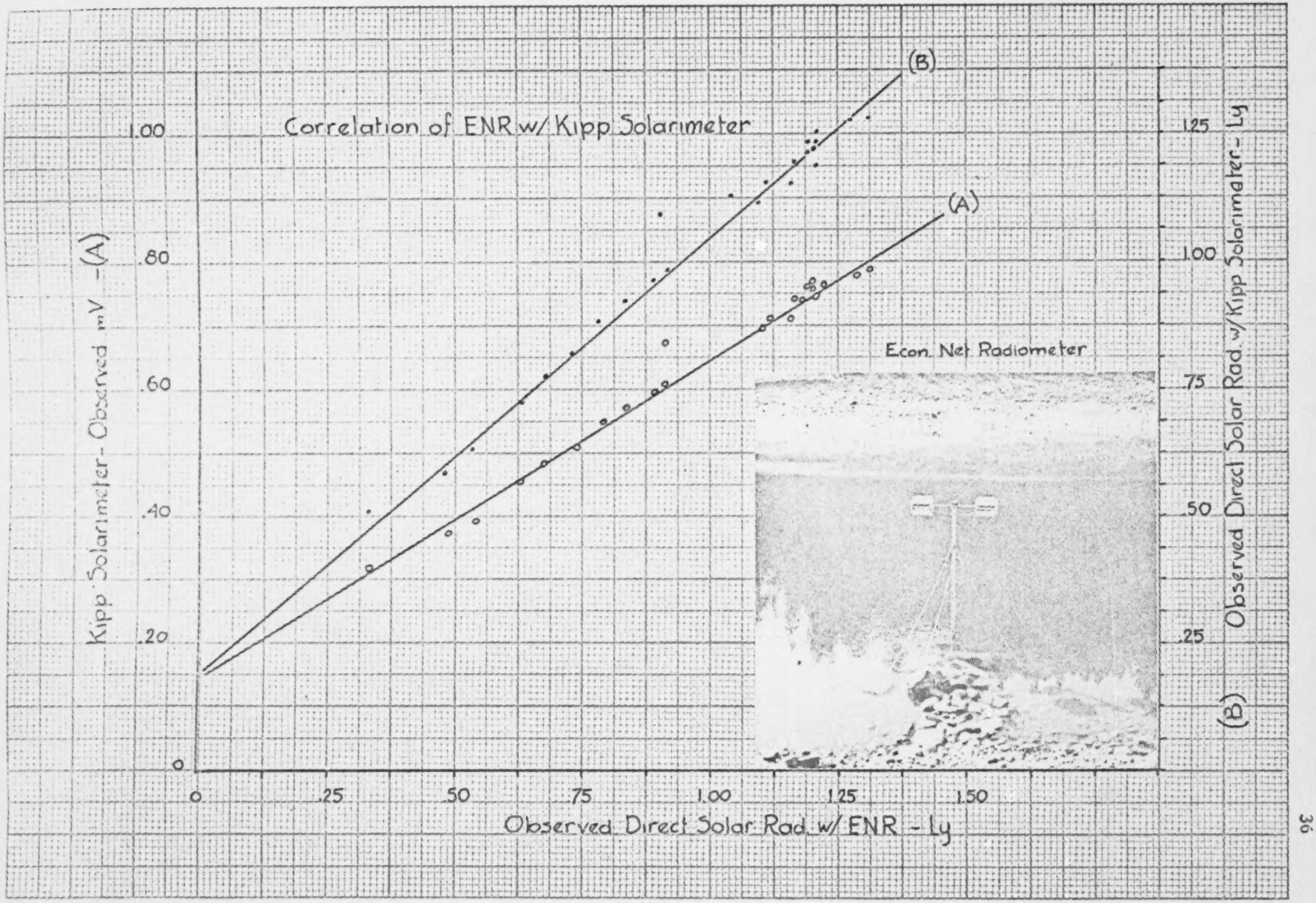
Correlation of ENR w/ Kipp Solarimeter
(B)
(A)
Econ. Net Radiometer
Kipp Solarimeter - Observed mV - (A)
(B) Observed Direct Solar Rad. w/Kipp Solarimeter - Ly
Observed Direct Solar Rad. w/ ENR - Ly
0
.25
.50
.75
1.00
1.25
1.50
.20
.40
.60
.80
1.00
1.25
.25
.50
.75
1.00

fig. 21

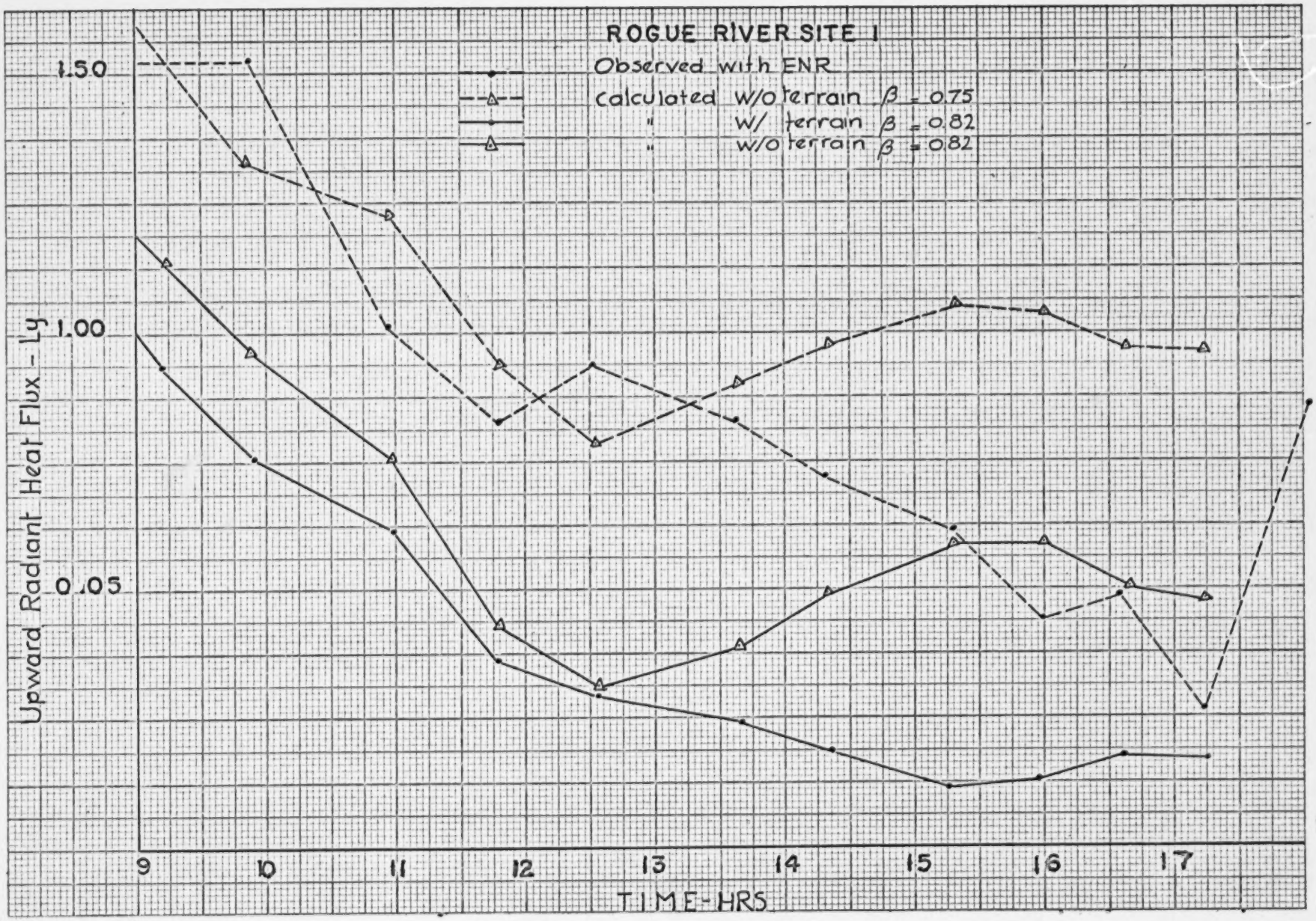
ROGUE RIVER SITE 1
Observed with ENR
Calculated W/O terrain β = 0.75
" W/ terrain β = 0.82
" W/O terrain β = 0.82
1.50
1.00
0.05
Upward Radiant Heat Flux - Ly
9
10
11
12
13
14
15
16
17
TIME-HRS

fig. 22

values of 0.75 and 0.82 and the third part is the longwave heat exchange between water and atmosphere disregarding terrain effects entirely and using equation 11 discussed in part 1 of this report. The curves were calculated from data taken in the field and tabulated in Appendix "B". Although the curves seem at first to have little in common several conclusions may be drawn.

It is evident that disregarding the terrain effects amounts over the entire daylight hours from 8 am to 5 pm to 0.0226 ly or 5 BTU/SF/HR which over a period of 9 hours amounts to 45 BTU/SF of river surface. Furthermore there is a close similarity between the back radiation pattern as observed with the ENR and the calculated values from the analog model describing this terrain. The reason for this lies in the selection of the β value (the atmospheric emissivity factor). No dependable values of this guantity are available for this area. Burt developed a set of curves which give a general relationship of β to vapor pressure. It is these curves which have been used. fig. 23. It appears however that the β value selected on the basis of site vapor pressure measurements is in error and that a value of 0.70 would be more accurate.

The terrain in this area does not appreciably affect the radiant heat pattern. A rate of 2 BTU/SF/HR is only about 1% of the incoming solar radiation and is hardly significant. After 1 PM the rocks and trees reach their maximum temperatures. Rocks become very much warmer than the air temperature while trees are at or near air temperature. Since in the Rogue River area rocks and trees are mixed on the slopes and mixed with grasses etc., the morning effect is mostly due to the fact that the trees although quite close to the air

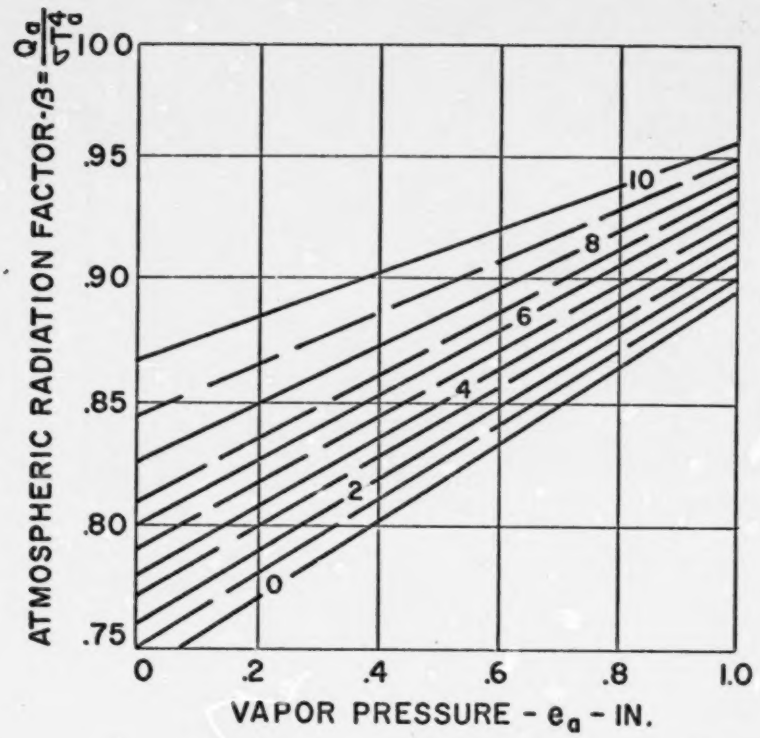

FIG.28
ATMOSPHERIC RADIATION FACTOR
(AFTER BURT)

temperature have an emissivity factor of ~ 95% and the air 70% - 75%. This causes the slight depression of the upward heat flux as shown between the curves representing with terrain and without terrain heat exchange for similar β values.

In the afternoon as the air temperature begins to drop off and the water temperature drop lags considerably behind, the effect of heat storage in trees and rocks shows up more dramaticially for now this radiant heat continues to depress the upward heat flow also contributing to keeping the air warmer and because of topography

essentially trapped in the canyons. If the terrain had not been present the back radiation would have been more efficient.

For canyons of the type through which the Rogue River flows it may be concluded from the data obtained that a slight depression of the back radiation may be expected in the morning on the order of 2-3 BTU/SF/HR and considerable (8-10) BTU/SF/HR back radiation depression during the afternoon. Estimates of back radiation ignoring terrain effects may thus be considerably in error.

The results obtained on one site on the Deschutes River are shown in fig. 24. The same type of curves are shown as for the Rogue River. There are different characteristics for terrain of this type which is almost void of any vegetation. See fig's. 20, 21, and 22. These sites were so chosen as to provide the greatest possible contrast in vegetation and still have comparable view factors.

All the curves are all similar in pattern. The ENR is a little more erratic but is still in general of the same conformity as the other curves.

The depression of back radiation as calculated from observed terrain temperature data is again noted. However due to the much colder temperature of the stream the curves are much lower than for the Rogue in the morning. The difference in stream temperatures is 10 to 15^{o} F. The uniformity of the heat flux depression is accounted for by the much more rapid heating of rock surfaces to much higher temperatures (especially the near vertical surfaces even during low sun elevation angles.) in the morning where as on tree and

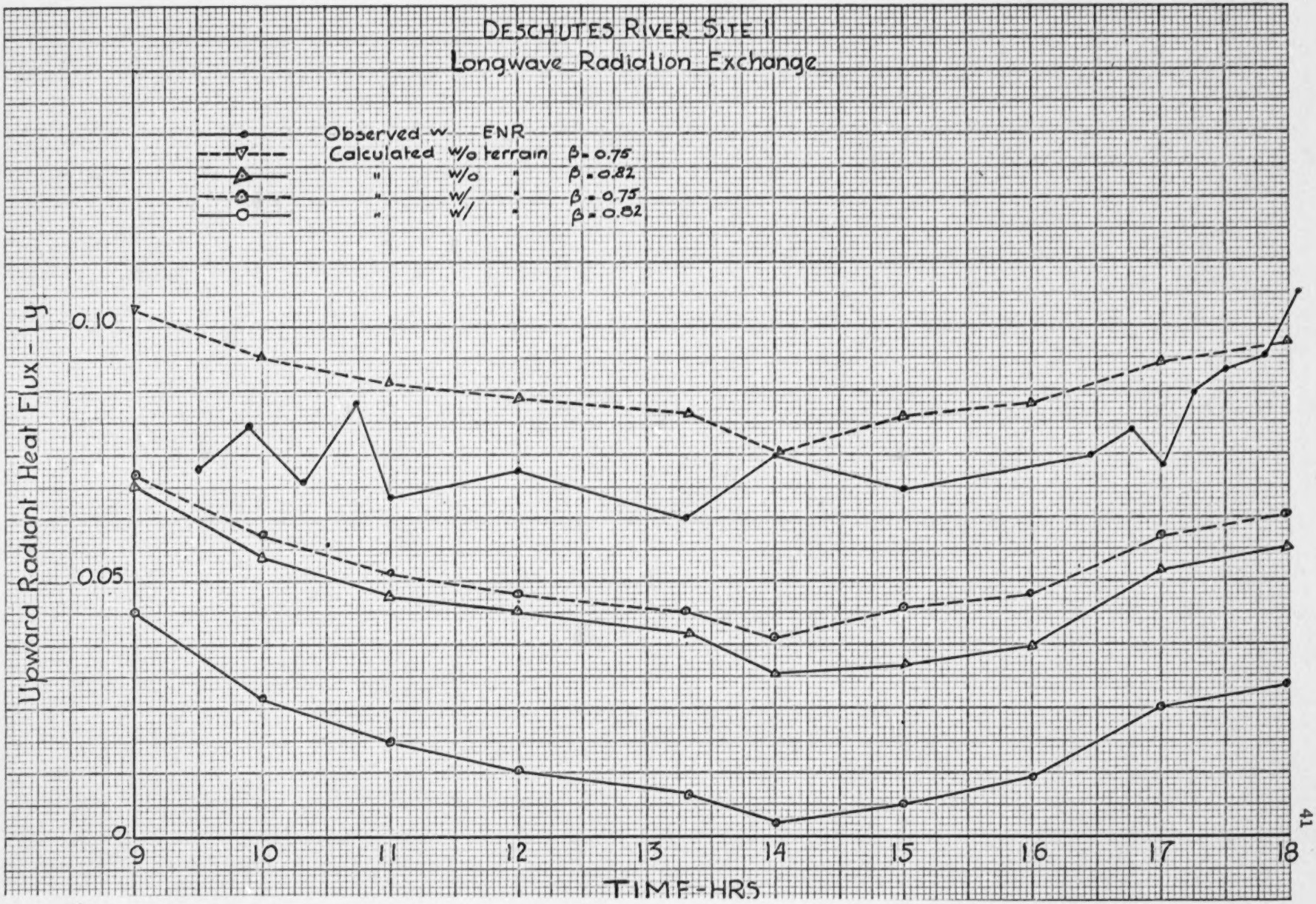
DESCHUTES RIVER SITE 1
Longwave Radiation Exchange
Observed w/ ENR
Calculated w/o terrain β = 0.75
" w/o " β = 0.82
" w/ " β = 0.75
" w/ " β = 0.82
Upward Radiant Heat Flux - Ly
0.10
0.05
0
9
10
11
12
13
14
15
16
17
18
TIME-HRS

fig. 24

vegetation covered surfaces the heat energy is diffused between leaves and grass.

Thus the effect here is on the order of 6-7 BTU/SF/HR during morning hours compared to 1-2 BTI/SF/HR for the vegetation covered slopes of the Rogue River.

. The continuing depression during the afternoon is due to the same reason that was mentioned for the Rogue River, the greater width and barreness of the canyon may provide for greater air circulation than in the narrow Rogue River canyons. There is therefore not divergence between curves representing heat exchange with and without terrain. It may be noted that the energy flux curve for the Rogue River does not start to increase until 5 PM while the energy flux pattern for the Deschutes River starts rising after 3 PM. The reasons which may cause this are that the Rogue at this point is very narrow and is almost until the very sunset exposed to solar radiation. The energy flux curves for the Deschutes site #1 and sites 3 and 4 on the Rogue all display the parallelism noted in fig. 22. These sites however were located more or less in the N-S stretch of the stream in much wider section and the rocks providing radiant heat were out of the direct rays of the sun much sooner than on site 1 on the Rogue where rocky walls were in the sun until much later in the afternoon at low solar angles thus retaining much more heat than North facing slopes which recieve the bulk of their heat load during the morning.

This appears therefore to be a characteristic of the site and of the energy flux pattern existent for that site.

CONCLUSIONS

Energy budget calculations for streams are not a new thing. However the state of the art is not well developed and many unknown factors remain. With the objective of determining the influence of terrain radiation it may be stated, that this factor does influence the energy budget sufficiently, that, for streams flowing through deep canyons having terrain elevation angles of 20^{o} or more, it is warranted to include the effects in the overall energy budget.

The extra energy budget calculations appear large. A stream side slope inventory must be made either from quadrangle map sheets or by making field measurements with a clinometer from a boat.

Also some average terrain temperature values must be known. These are not as difficult to obtain as may appear. A series of flights with a Bendix Thermal Mapper will provide excellent terrain temperature data. A short study of average terrain temperature values may suffice. Once this information is available the use of the analog model to set up the matrix of simultaneous equations on a digital computer provides the solution at very low cost.

Terrain surrounding a stream is thus a detriment to the back radiation factor which is part of the stream' cooling mechanism, by depressing the back radiation value to a magnitude of 45 BTU's/SF/ to 75 BTU/SF per 10 hour day light period and probably also during the night to the same or greater extent.

The difficulty of obtaining accurate β values is and remains of prime concern to investigators handling atmospheric radiation problems.

THE GEOMETRY OF STREAMS AND THE EFFECT OF SHADING

Although there are very few straight streams yet even meandering streams have a predominant direction of travel for extensive stretches during which a stream may be said to be flowing primarily North, North East, etc. Such streams when surrounded by steep terrain or trees are shielded from early morning and late afternoon sun even during the middle of the summer. The object is to determine how much solar radiation is eliminated for a stretch of stream having one of 6 major azimuth directions: 270, 300, 330, 0, 30, and 60. The remaining directions are back Azimuths and therefore present the same problem.

The average amount of solar radiation received per day for the entire year and country is 300 langleys. The amount varies from 100 to 800 langleys depending on season and region. The following tabulation gives average daily amounts of solar radiation received regionally over the United States on a unit horizontal surface for each month of the year. This table is prepared by the U.S. Weather Bureau (1964).

	Northeast	Southeast	Midwest	Northwest	Southwest
January	125	200	200	150	275
February	225	275	275	225	375
March	300	350	375	350	500
April	350	475	450	475	600
May	450	550	525	550	675
June	525	550	575	600	700
July	525	550	600	650	700
August	450	500	525	550	600
September	350	425	425	450	550
October	250	325	325	375	400
November	125	250	225	175	300
December	125	200	175	125	250

Average Solar Radiation Values
received in different parts of the U.S.
Table 5

Latitudinal effects are most pronounced in the fall and early winter; there is little variation in the amounts received during the summer. The greater values for the Southwest result from the relatively sparse cloud cover over the area.

The rate of in coming solar radiation for an instant of time at a given day of the year at a specified latitude is given by $I_i = I_n$ $(\sin\phi \sin\delta_s + \cos\phi \cos\delta_s \cos t.)$ (18)

where the quantity between parenthesis is the cos z or the zenith angle of the sun. ϕ = Latitude

δ_s = Solar declination from an ephemeris

t = hour angle of the sun from noon to AM or PM

$I_n = I_o \tau_a^m$

I_o is the solar consant or 442 BTU/SF/HR = 2 ly

τ_a = is the atmospheric absorption factor which depends on dust, moisture, CO_2, etc. $_a$ = 0.62 for clear days--0.81 for cloudy days, τ_a = 0.7 is considered an acceptable average. m is the relative air mass. i.e. the ratio of the actual path and the shortest possible path. For all practical purposes: m = Secant Z. Tabulated values for m are taken from Technical Bulletin No. 1344, U.S. Dept. of Agriculture and are shown in Table 6.

Elevation of sun	Relative path length (optical airmass)	Extraterrestrial intensity on a surface: Perpendicular surface (percent)	Extraterrestrial intensity on a surface: Horizontal surface (percent)
90°	1.00	78	78
80°	1.02	77	76
70°	1.06	76	72
60°	1.15	75	65
50°	1.31	72	55
40°	1.56	68	44
30°	2.00	62	31
20°	2.92	51	17
10°	5.70	31	5
5°	10.80	15	1
0°	45.00	0	0

Table 6

Equation (18) may be used to calculate the solar radiation intensity received at any time of the day and knowing the intensities the accumulated radiation may be calculated. Not all radiation received at a horizontal surface is direct; part of the radiation is diffuse as shown in Table 7.

Solar altitude,	Standard Cloudless Atmosphere: Direct, perpendicular (ly/min)	Diffuse on Horizontal (ly/min)	Total on Horizontal (ly/min)	Direct perpendicular (BYU/SF/HR)	Diffuse on Horizontal (BYU/SF/HR)	Total on Horizontal (BYU/SF/HR)
5.....	0.30	0.03	0.06	65	6	13
10.....	.56	.06	.16	123	13	35
20.....	.89	.10	.41	196	22	90
30.....	1.06	.13	.66	234	29	146
40.....	1.17	.14	.89	258	34	197
50.....	1.24	.15	1.09	274	33	241
60.....	1.28	.15	1.26	283	33	279
70.....	1.31	.16	1.39	289	35	308
80.....	1.32	.16	1.46	291	35	323
90.....	1.33	.16	1.48	293	35	328

Solar Radiation for Clear Atmosphere
in langley/minute and BTU/SF/HR.
Adapted from Brooks 1959)

Table 7

The difference between total radiation and diffuse radiation is the amount which can effectively be shaded or blocked out by terrain. This direct solar radiation is further reduced by reflectivity which is dependent on solar altitude and cloud cover, figures 25 and 26. The composit direct solar radiation intensity as a function of solar altitude corrected for diffuse radiation and reflectivity is shown in fig. 27 for a clear sky.

The object is to determine how much radiation does not reach the water surface because of the effective blocking by terrain.

It is required then to determine the solar altitude at which the sun just appears over the terrain for a stream of axiauth , latitude $\emptyset$ and terrain elevation determined by an angle β° which is taken at the center of the stream from the horizontal plane to the top of the terrain perpendicular to the stream, on a specific day of the year, and the horizontal (time) angle when the sun just appears at solar altitude h_a.

The variables are then $h_a = f(\emptyset, \delta_s, \alpha, \beta^{\circ})$

h_a = solar altitude

$\emptyset$ = latitude

δ_s = average solar declination for specific day

α = azimuth of the stream

β° = terrain angle

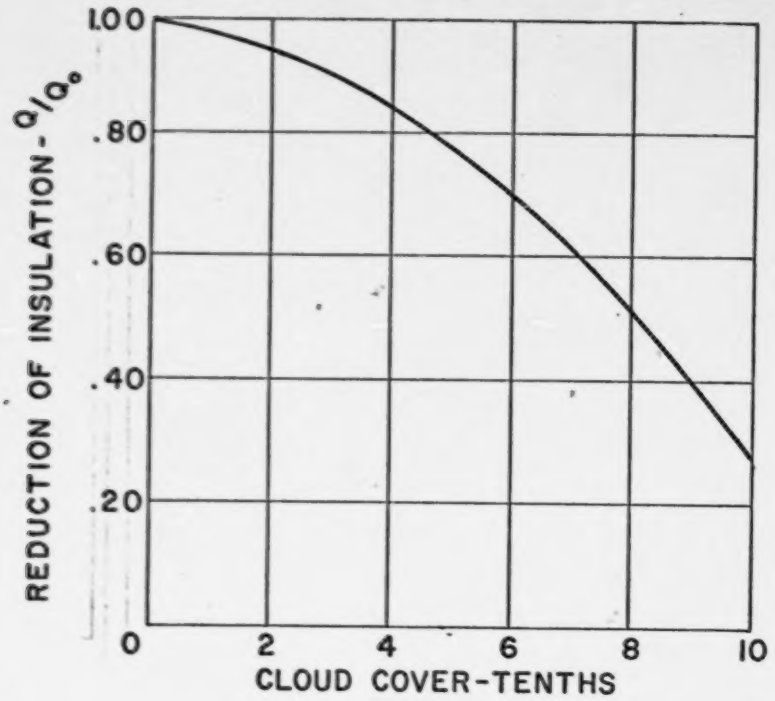

FIG.25
EFFECT OF CLOUD COVER ON INSULATION

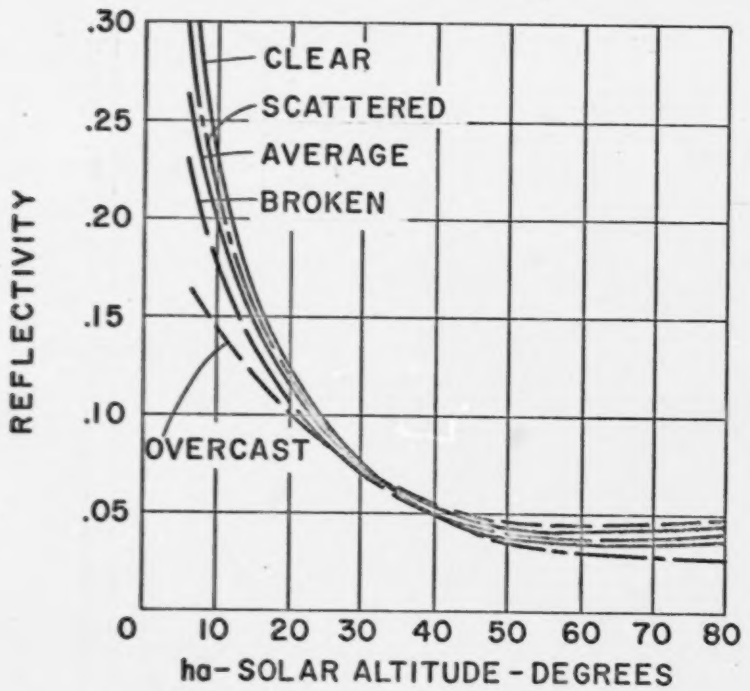

FIG.26
EFFECT OF SOLAR ALTITUDE AND CLOUD COVER
ON REFLECTIVITY

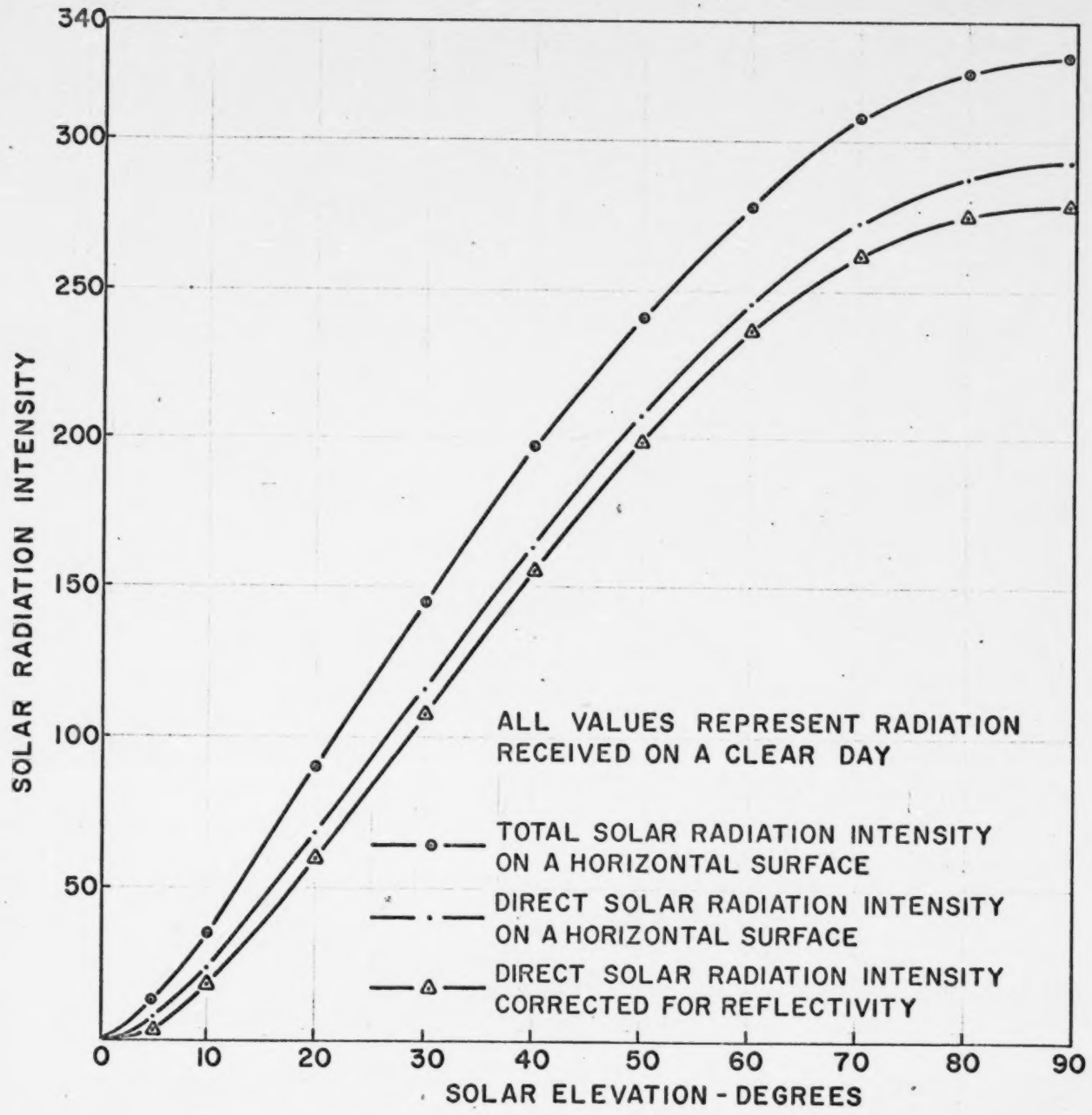

FIG. 27
SOLAR ALTITUDE VS RADIATION INTENSITY

A section of a stream is considered as having an Azimuth α in the NE Quadrant. The geometry of such a case is shown in fig. 28

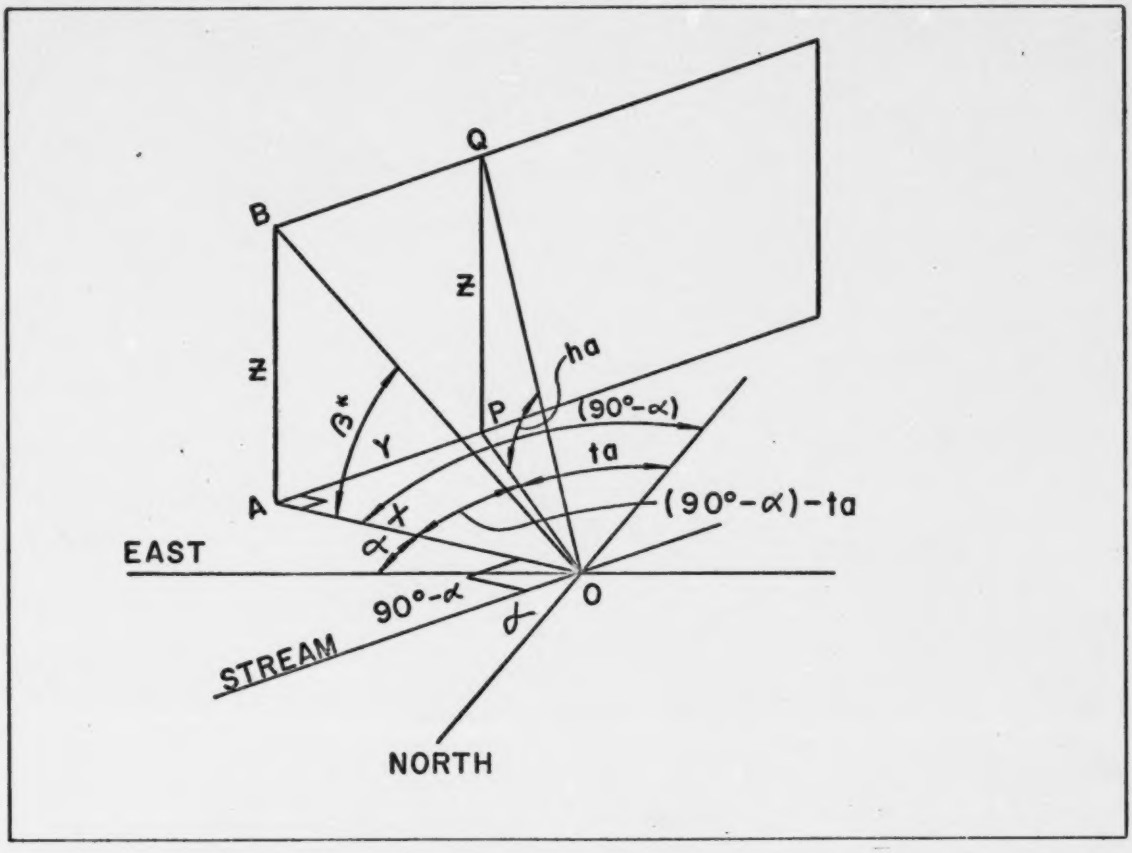

FIG. 29
GEOMETRY OF SHADING IN N. E. QUADRANT

In $\triangle$OAB

$$\tan \beta^* = \frac{Z}{x} \qquad Z = x \tan \beta^*$$

In $\triangle$ OAP

$$\cos \left[(90-\alpha)-t_a\right] = \frac{x}{OP} \qquad OP = \frac{x}{\cos \left[(90-\alpha)-t_a\right]}$$

We want h_a the vertical angle at the time the sun just appears over

the horizon.

$$\tan h_a = \frac{PQ}{OP} = \frac{Z}{\frac{x}{\cos\ (90-\alpha)-t_a}}$$

substituting and cancelling

$$\tan h_a = \frac{x \tan \beta^*}{\frac{x}{\cos\left[(90-\alpha)-t_a\right]}}$$

$$\tan h_a = \tan \quad \cos\ (90- \quad)-t_a$$

from equation (1) we see that

$$\sin h_a = \cos Z_a = \sin\phi \sin\delta_s + \cos\phi \cos\delta_s \cos t_a$$

if we set $\sin\phi \sin\delta_s = C_1$

and $\cos\phi \cos\delta_s = C_2$

then

$$\sin h_a = C_1 + C_2 \cos t_a$$

$$\cos t_a = \frac{\sin h_a - C_1}{C_2} = \frac{\sin h_a}{C_2} - \frac{C_1}{C_2}$$

set

$$\frac{1}{C_2} = C_3$$

$$-\frac{C_1}{C_2} = C_4$$

then

$$\cos t_a = C_3 \sin h_a + C_4$$

$$\sin t_a = \left[1 - (C_3 \sin h_a + C_4)^2\right]^{\frac{1}{2}}$$

Expanding equation (3)

$$\tan h_a = \tan \beta^* \left[\cos t_a \cos (90-\alpha) + \sin t_a \sin (90-\alpha)\right]$$

$$\tan h_a = \tan \beta^* \left[\left(C_3 \sin h_a + C_4\right) \sin\alpha + \left[1 - (C_3 \sin h_a + C_4)^2\right]^{\frac{1}{2}} \cos\alpha\right] \qquad (19)$$

In this expression only h_a is unknown and this may be solved by iteration using a digital computer.

A set of curves reflecting the variation of h_a with latitude ϕ, Azimuth angle α, shading angle β^* and, for specific days, the average declination of the sun are shown in fig's 31,32 for latitude 45°.

For North and East directions $\alpha = 0, 90$ and the equations become:

for North $\alpha = 0$ $\quad \tan h_a = \tan \beta^* \left[1-(C_3 \sin h_a + C_4)^2\right]^{\frac{1}{2}}$

for East $\alpha = 90^\circ$ $\quad \tan h_a = \tan \beta^* \left[(C_3 \sin h_a + C_4)\right]$

The geometry for the NW Quadrant is shown in fig. 29

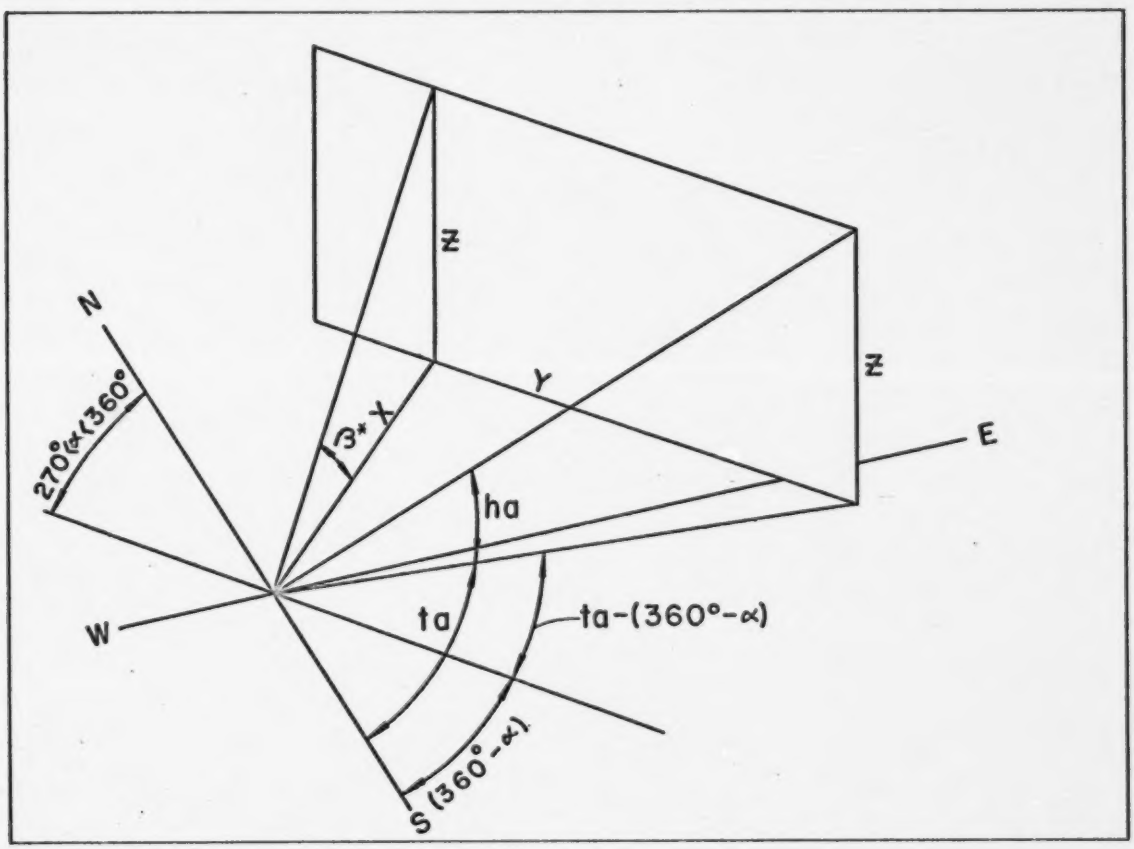

FIG. 30
GEOMETRY OF SHADING IN N. W. QUADRANT

In Δ OAB

$$\tan \beta^* = \frac{Z}{x} \qquad Z = x \tan \beta^*$$

In Δ OAP

$$\sin \left[t_a - (360 - \alpha) \right] = \frac{x}{OP} \qquad OP = \frac{x}{\sin \left[t_a - (360 - \alpha) \right]}$$

In Δ OPQ

$$\tan h_a = \frac{Z}{OP} = \frac{x \tan \beta}{\frac{x}{\sin \left[t_a - (360 - \alpha) \right]}} = \tan \beta \left[\sin (t_a - (360 - \alpha)) \right]$$

remembering that

$$\cos t_a = C_3 \sin h_a + C_4$$

$$\sin t_a = 1 - (C_3 \sin h_a + C_4)^2 \quad \frac{1}{2}$$

Expanding

$$\tan h_a = \tan \beta^* \left[\sin t_a \cos (360 - \alpha) - \cos t_a \sin (360 - \alpha) \right.$$

$$\tan h_a = \tan \beta^* \left[+\sin t_a \, (+\cos \alpha) - (\cos t_a)(-\sin \alpha) \right.$$

$$\tan h_a = \tan \beta^* \left[(1 - (C_3 \sin h_a + C_4)^2)^{\frac{1}{2}} \cos \alpha + \right.$$

$$\left. (C_3 \sin h_a + C_4) \sin \alpha \right] \qquad (20)$$

When $\alpha = 90^\circ$ $\qquad \cos \alpha = 0$

$$\sin \alpha = 1$$

Thus for West or East flowing stream or $\alpha = 90^\circ$

$$\tan ha = +\tan \beta^* \, (C_3 \sin h_a + C_4) \qquad *$$

for North or South flowing stream or $\alpha = 180^\circ$

$$\cos 180 = -1$$

$$\sin 180 = 0$$

$$\tan h_a = \tan \beta^* \left[(1 - (C_3 \sin h_a + C_4)^2 \right]^{\frac{1}{2}}$$

* It may happen for low angles h_a that tan h_a is negative.

The negative sign may seem to be confusing for how can h_a ever be negative. The answer lies in the fact that there is a relationship between h_a and t_a and t_a is $>$ 90 for low angles of h_a. The constants C_3 and C_4 assume cos t_a to be positive, so in cases of low h_a, C_3 and C_4 reverse signs. In the solution this appears as a negative value for tan h_a.

The general equation 19, 20 is somewhat laborious to handle unless a computer is employed to obtain h_a, t_a values. Therefore a set of curves may be generated using a simple analog model of the following construction, fig. 30.

A sheet of 2 ft. x 2 ft. plywood was used as the base. On one edge in the middle a 90° protractor was attached. A hole drilled in the radius center of the protractor into the plywood and on the opposite side of the sheet of plywood positions the solar plane. A piece of galvanized wire was bent into s semi-circle and 90° angles on the ends. The ends were set into the holes so the plane of the sun's movement is defined by the wire for any inclination with the horizon plane. The specific value may be read off to the nearest half degree on the protractor.

In the center, a lower and upper circular plate with degree divisions were placed on top of each other, the lower being about 2 inches in diameter larger, in such a way as to permit the upper plate to rotate. Another half of a protractor was erected on the upper plate with its arc toward the 0° mark or North on the upper plate.

A movable rectangular piece of plywood (4" x 18") with foot pieces to allow it to be set on the vase in any azimuth direction

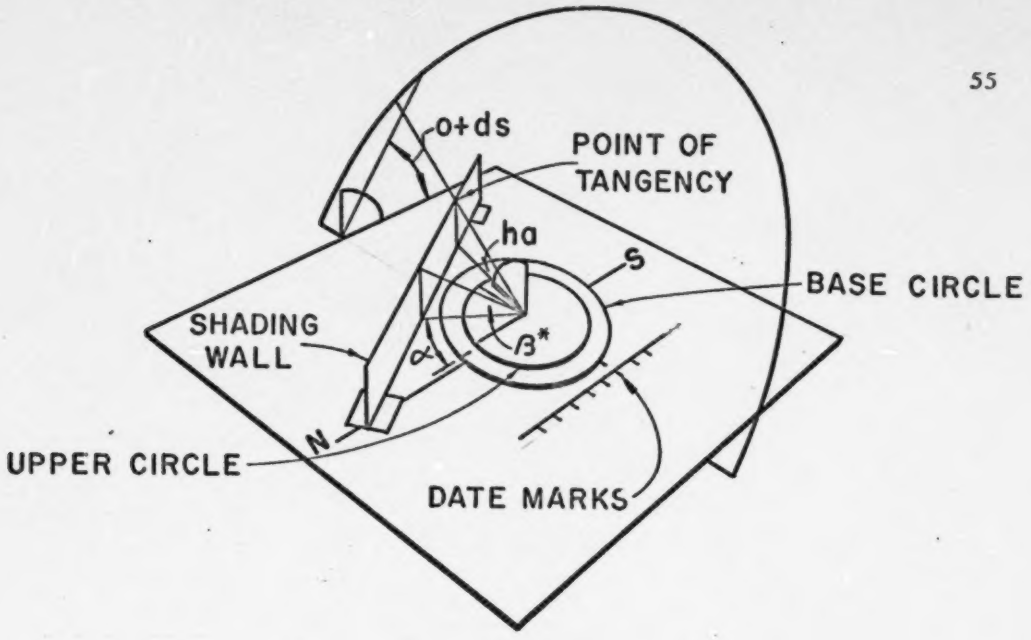

FIG.34
SOLAR SHADING MODEL

functioned as the terrain providing the shade. A slot was cut on the bottom so this analog shading advice could be placed near the center protractor on the upper plate.

The model is deficient in that it does not reflect the horizontal sunrise angles faithfully due to the smallness of scale. The model assumes a point position for earth and thus introduces a small error by ignoring the horizontal sunrise position. Calculations indicate this problem to be of minor significance. See Appendix "C".

It was required to find the solar elevation for a specific day D at Latitude Ø at which the sun will just come over the terrain of perpendicular shading angle β^*. (β^* is determined perpendicular to the stream assuming the terrain contributing to shading to be parallel to the stream.)

This arrangement permits the observation and positioning of all angles and directions which are part of the problem.

The solar angle may be set with the wire and the direction of stream flow and thus the shading angle by an azimuth direction of the 0° mark of the upper plate on the lower plate.

After positioning the terrain (shading device) parallel to the stream and perpendicular to the protractor a string is stretched from the center of the plates to the solar path (circular wire) while just touching the terrain (shading device). The upper plate is then rotated until the upright protractor just touches the string. The vertical angle read along the string is very close (1°) to the vertical angle of the sun appearing over the horizon.

The values of the vertical angles thus obtained are plotted as functions of α and β^{*}, fig's. 31,32. Checks between analog model and equation 19, 20 are shown in Appendix "C".

Families of h_a curves for several days of the year for a latitude may be combined in a single figure, however for other latitude values a new set of curves must be generated.

With the h_a angles thus obtained the solar radiation being blocked out must be determined.

The radiation pattern and distribution is unique for any latitude and date. It is therefore necessary to obtain the solar radiation distribution with time for a specific day. The manner of obtaining this has been explained earlier. However a short explanation follows and a typical set of calculations is given in Appendix "D".

First the angular length of the visible solar orbit at a given place and date is found from

$$\sin h_a = \sin \phi \sin \delta_s + \cos \phi \cos \delta_s \cos t_a$$

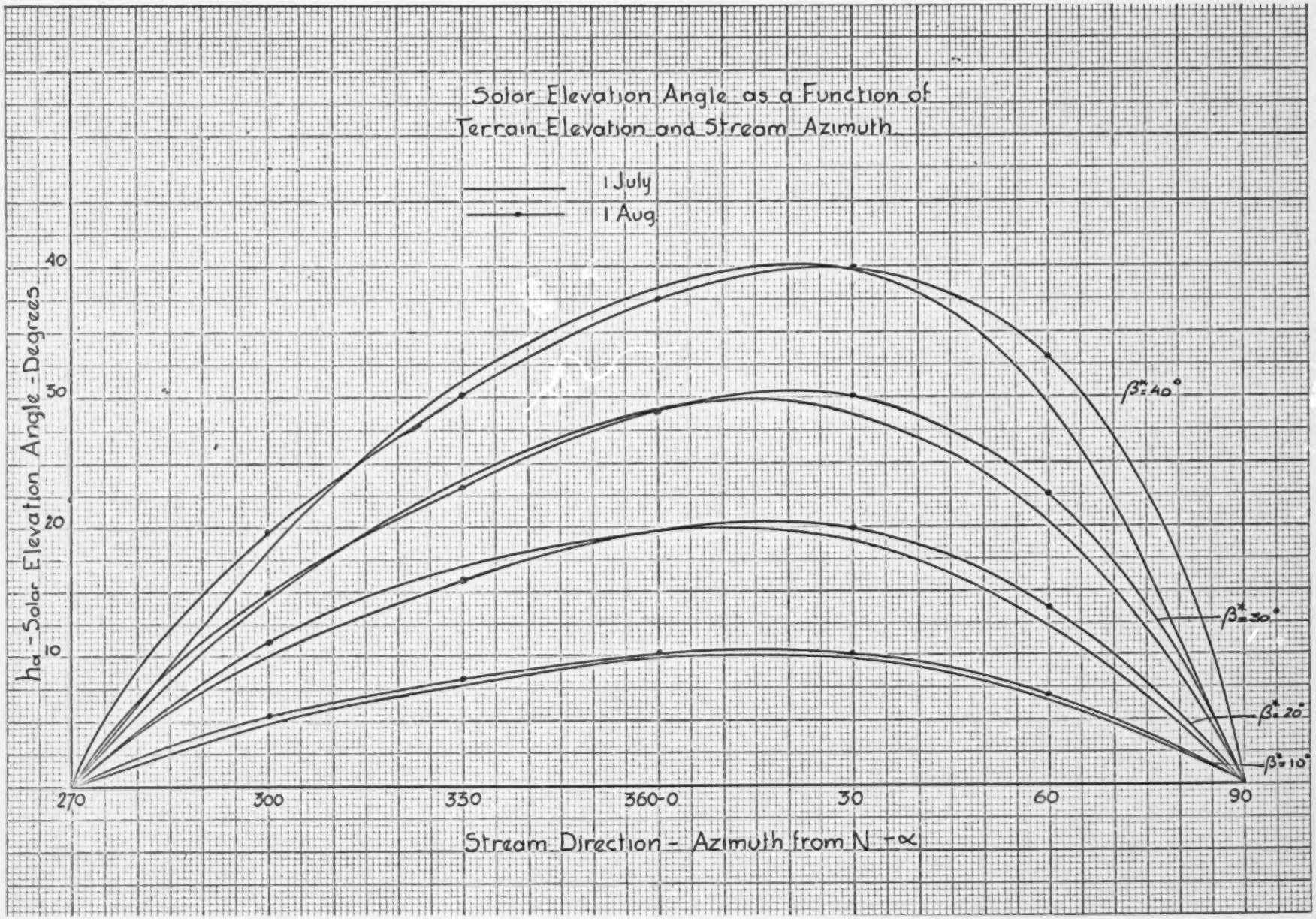
Solar Elevation Angle as a Function of
Terrain Elevation and Stream Azimuth
1 July
1 Aug.
h_α - Solar Elevation Angle - Degrees
40
30
20
10
$\beta^* = 40°$
$\beta^* = 30°$
$\beta^* = 20°$
$\beta^* = 10°$
270
300
330
360-0
30
60
90
Stream Direction - Azimuth from N - α

fig. 31

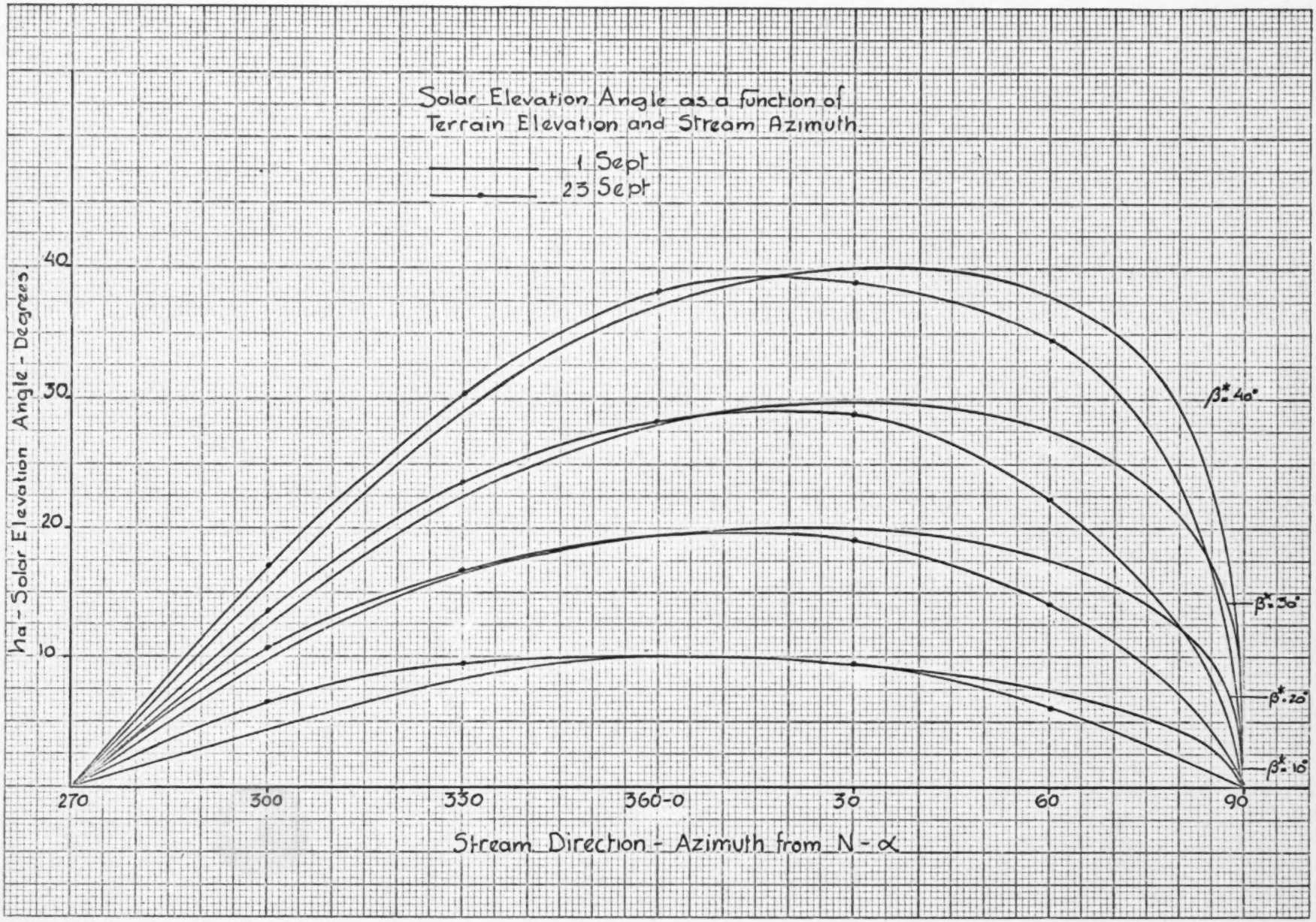
Solar Elevation Angle as a function of
Terrain Elevation and Stream Azimuth.
1 Sept
23 Sept
ha - Solar Elevation Angle - Degrees
40
30
20
10
β*.40°
β*.30°
β*.20°
β*.10°
270
300
330
360-0
30
60
90
Stream Direction - Azimuth from N - α

Fig. 32

since at sunrise $h_a = 0$

$$\cos t_a = \frac{-\sin \phi \sin \delta_s}{\cos \phi \cos \delta_s}$$

and from this value t_a may be found.

The hour length of a solar day may be calculated by dividing this value by 15° and multiplying by two (2).

The values of the length of a solar day for several specific days and latitudes and the azimuth of sunrise for these days have been tabulated in Table 8.

Length of Solar Day for Dates and Latitudes

Date	Lat. ϕ degrees	δ_s	t_a @ sunrise or sunset degrees Equatorial Plane	$\frac{1}{2}$ Solar day Hours	Solar Day Hours L. rounded to .1
1 June	45°	22° 2'	113 53	7.6	15.2
16 June	45°	23° 21'	115 28	7.69	15.4
1 July	35°	23° 04'	107 24	7.16	14.3
	45°		115 17	7.63	15.3
	55°		127 27	8.5	17.0
16 July	35°	21° 31'	106 08	7.00	14.0
	45°		113 12	7.55	15.1
	55°		124 40	8.29	16.6
1 Aug	35°	17° 51'	103 03	6.87	13.7
	45°		108 27	7.22	14.4
	55°		117 20	7.82	15.6
16 Aug	35°	13° 22'	99 40	6.54	13.1
	45°		103 53	6.91	13.8
	55°		110 07	7.34	14.7
1 Sept	35°	8° 02'	95 40	6.37	12.7
	45°		98 10	6.54	13.1
	55°		101 07	6.74	13.5
23 Sept	35°	0	90 00	6.00	12.0
	45°		90 00	6.00	12.0
	55°		90 00	6.00	12.0

Table 8

Fig. 33 presents this same information in graphical form so that rapid interpolation for other dates and latitudes may be made.

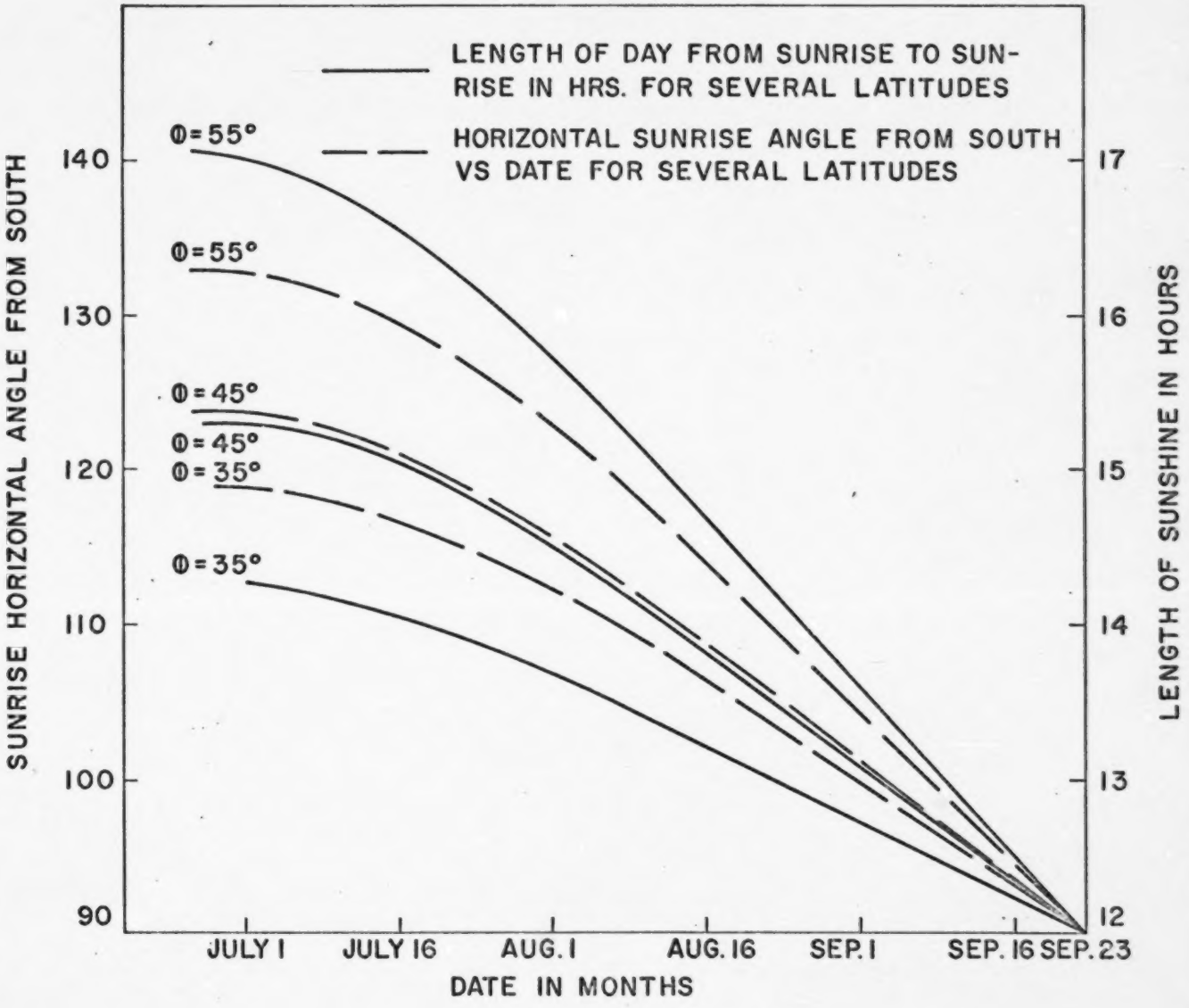

FIG. 35

The solar distribution for specific days and latitudes is found by calculating the solar elevation at even hour positions from apparent noon or the south position of the sun. Then using fig. 27 which gives the direct solar radiation on a horizontal surface as a function of altitude angle above the horizon the distribution of the incoming solar radiation is obtained. Summing the average values per hour, the accumulated solar radiation is calculated as a function of time. Then on the same plot the elevation angles of the sun are plotted as a function of the accumulated solar radiation received. This relationship is shown in fig. 34 for latitude 45° and six dates. An example of the solar radiation blocking is shown in the Kipp Solarimeter Graph in fig. 35. An example of making use of this information is shown below for that part of the Deschutes River in the Sinamox Quadrangle (fig's. 36 and 37) which is the area in which the test site were located. The data is found in Appendix "E".

The river was divided into reaches in two ways. First in ¼ mile reaches and then in reaches as determined by straight sections.

The crossection in the middle is determined from the Quadrangle map sheet on a one to one scale for each bank. The breakpoint on the slope determines the β' angle as viewed from the middle of the stream. The azimuth of the center line of the stream is measured to the nearest degree or half degree in the NW or NE quadrant.

With these α and β' angles the curves of fig. 34 are used to find h_a, the angle at which the sun appears over the terrain.

The h_a angle is then used in fig. 34 for the desired date to find the solar radiation blocked out by the stream.

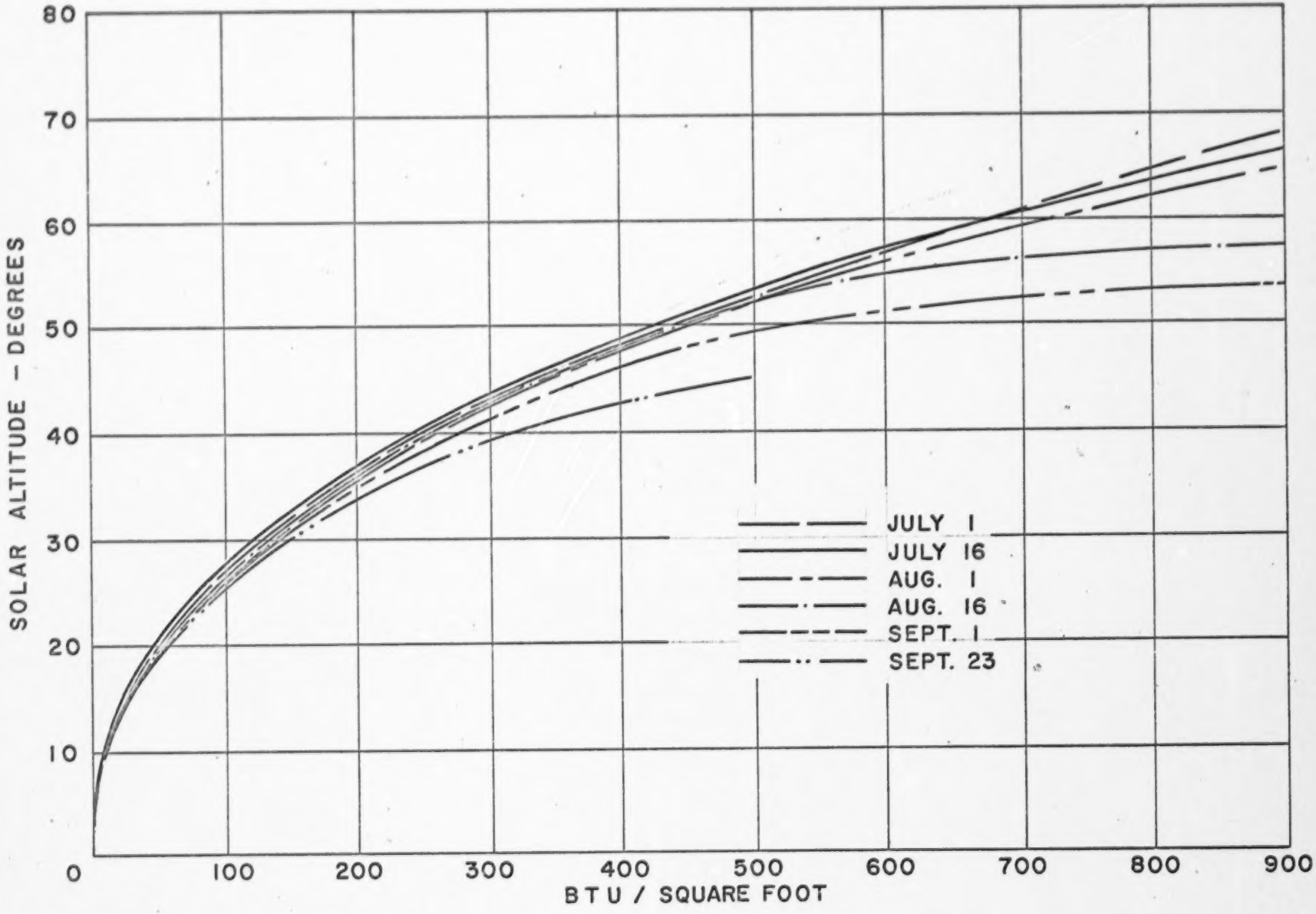

FIG. 37

ACCUMULATED SOLAR RADIATION FOR LAT. 45°

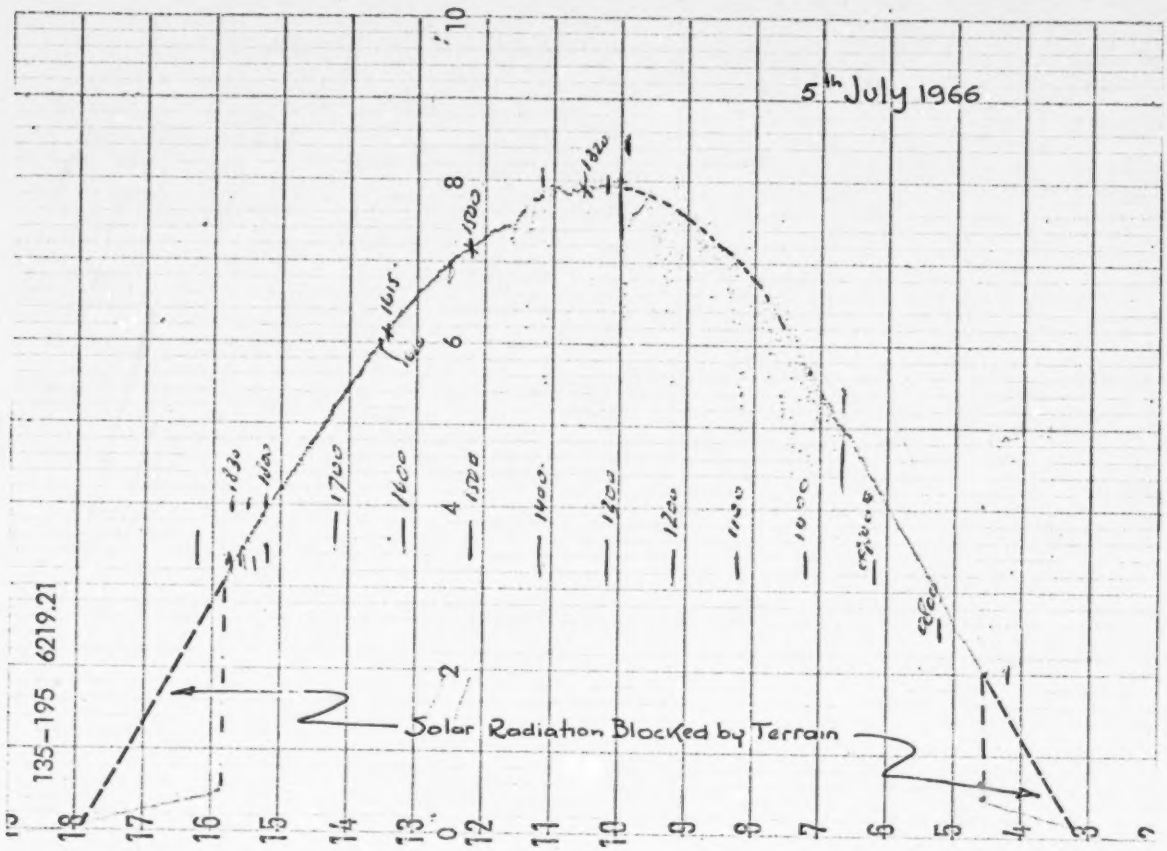

Solar Radiation Curve

fig. 35

For the Deschutes River in the Sinamox Quadrangle the following results were obtained:

¼ mile reaches	Solar Radiation blocked per day	52.3 BTU/SF
Straight reaches	Solar Radiation blocked per day	33 BTU/SF

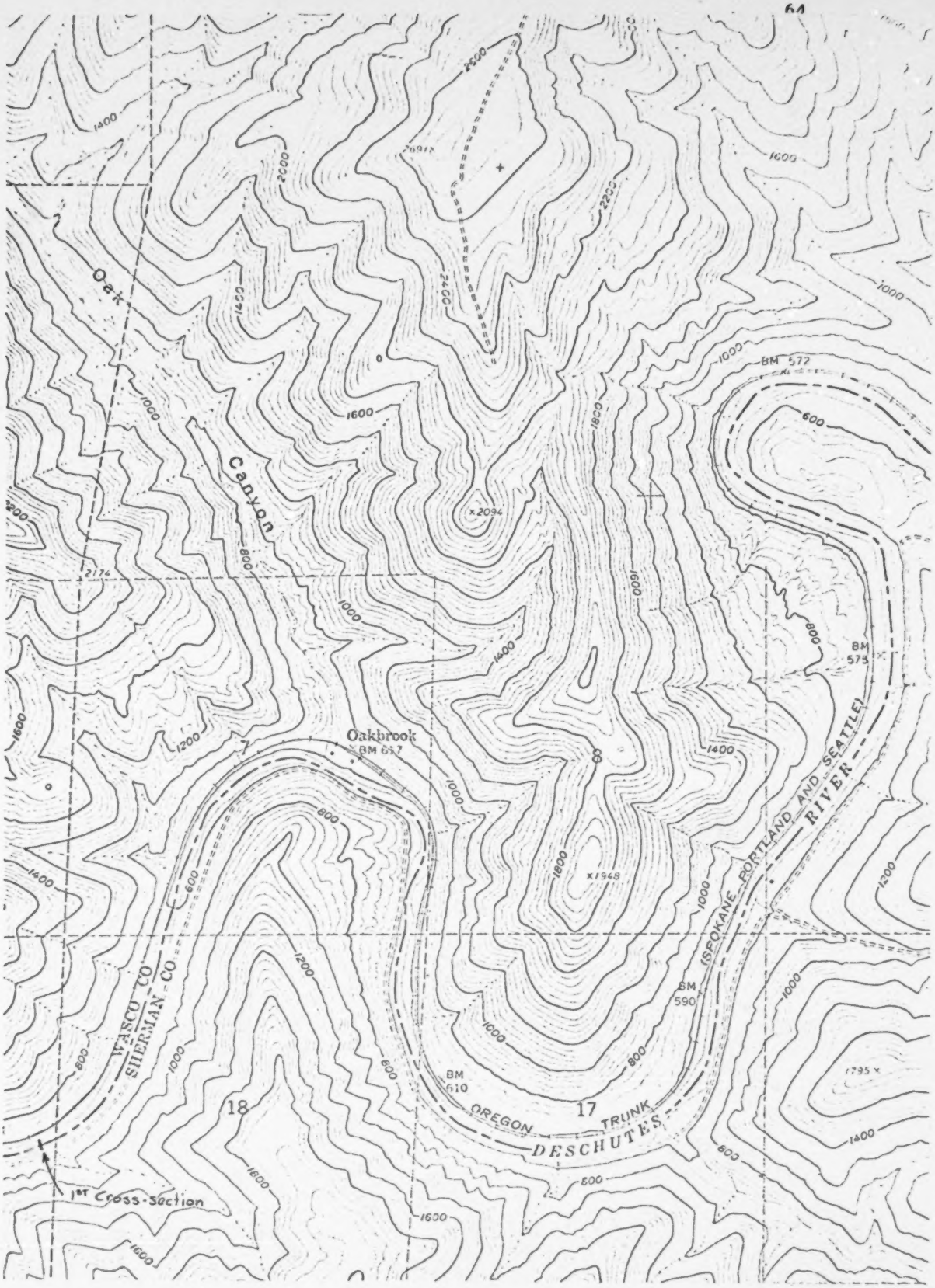

FIG. 40

SELECTION OF DESHUTES RIVER SINAMOX QUADRANGLE (7½')

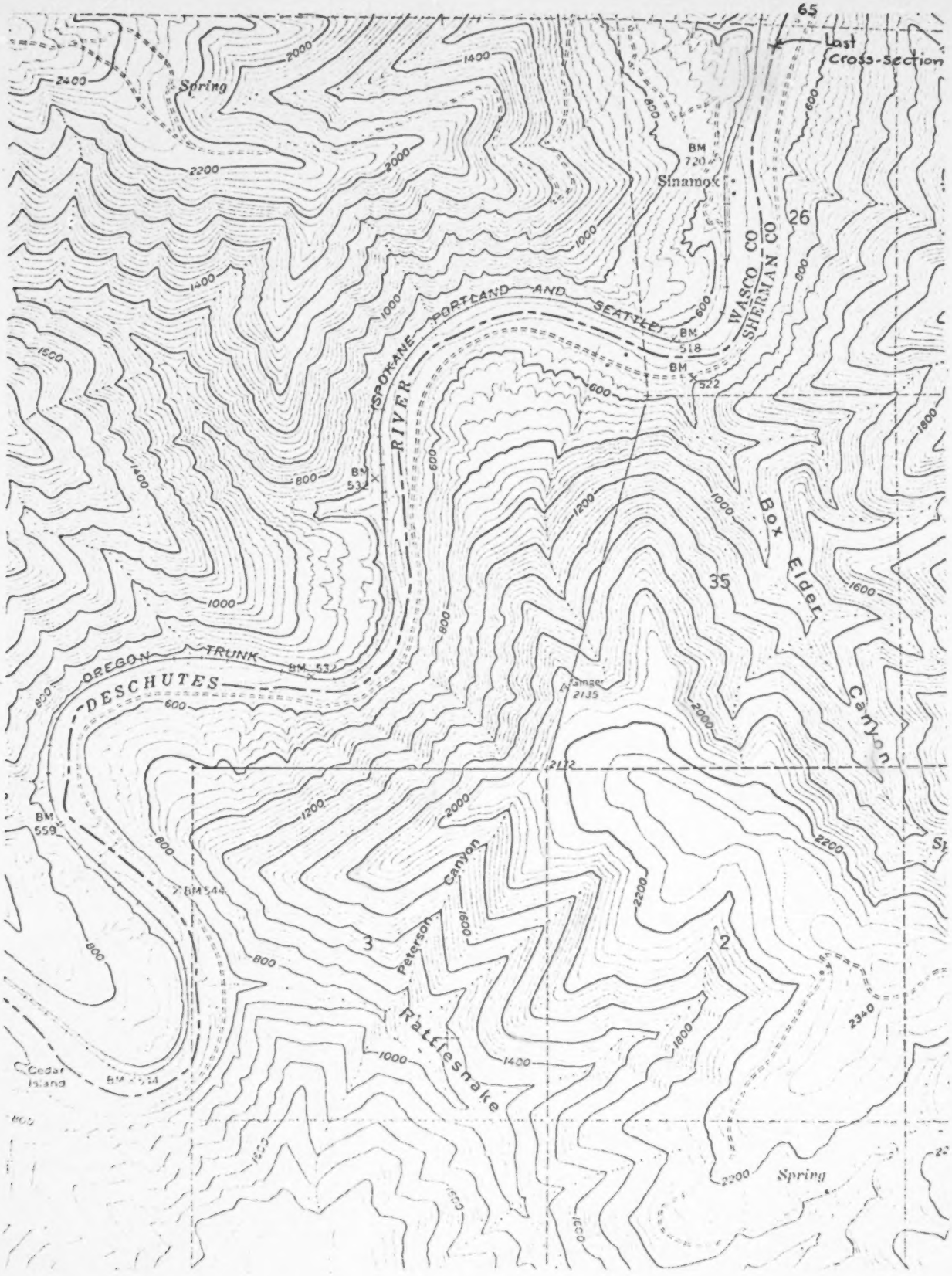

FIG. 39

SELECTION OF DESHUTES RIVER SINAMOX QUADRANGLE ($7\frac{1}{2}'$)

CONCLUSION

Terrain having elevation angles of 15° or more may be profitably examined for its effect upon reduction of solar radiation. An equation for determining the sun's elevation may be programmed on a digital computer as may the relationship of this angle with the accumulated solar radiation quantity. The effects of terrain shading will be especially important for the multitude of small tributary streams which are generally in a deep gully and have considerable vegetative cover. Experiments determining the effect of total vegetative shading showed that for such conditions 90 - 95% of the solar radiation was shielded out.

For streams such as the Deschutes and Rogue Rivers it would appear that the beneficial effect of shading by terrain of short-wave solar radiation is effect by the longwave heat exchange from the same terrain.

It is therefore concluded here that for most streams which have a width of 200 feet or greater the benefits offset the losses for the greatest part or vice versa.

There is however for streams with heavy bank growth a very great deal of benefit from the shading effects. Large scale aerial photographs of the stream should provide all the necessary information for the initial study to determine if the effects of shading should or should not be considered in a stream temperature study.

Appendix "A" Integration of View Factor Functions

Integration of the Function:

$$\frac{1}{\pi}\int_{-\infty}^{+\infty}\int_{\theta''}^{\theta'}\rho^3\,\frac{\cos\theta\,d\theta\,dy}{(\rho^2+y^2)^2}$$

first with respect to θ

$$\frac{1}{\pi}\int_{-\infty}^{+\infty}\frac{\rho^3\,dy}{(\rho^2+y^2)^2}\qquad \sin\theta\Big|_{\theta''}^{\theta'}$$

The integral form for this expression is

$$\int\frac{dx}{(ax^2+c)^n}=\frac{1}{a(n-1)c}\cdot\frac{x}{(ax^2+c)^{n-1}}+\frac{2n-3}{2(n-1)c}\int\frac{dx}{(ax^2+c)^{n-1}}$$

if a=1, c= ^{2}, n=2, and x=y

Then

$$\int\frac{dy}{(\rho^2+y^2)^2}=\frac{1}{2(2-1)\rho^2}\cdot\frac{y}{(y^2+\rho^2)^{2-1}}+\frac{2(2)-3}{2(2-1)}\,2\int\frac{dy}{(y^2+\rho^2)^{2-1}}$$

$$=\frac{1}{2\rho^2}\cdot\frac{y}{y^2+\rho^2}+\frac{1}{2\rho^2}\int\frac{dy}{(y^2+\rho^2}$$

The integral of $\int\frac{dy}{y^2+\rho^2}=\frac{1}{\sqrt{\rho^2}}\tan^{-1}\left(y\sqrt{\frac{a_1}{2}}\right)$

using the integral form $\int\frac{dx}{ax^2+c}=\frac{1}{ac}\tan^{-1}\left(x\sqrt{\frac{a}{c}}\right)$

Thus the final expression to be evaluated between $\pm$ is

$$=\frac{\rho^3}{\pi}(\sin\theta'-\sin\theta'')\left(\frac{1}{2\rho^2}\cdot\frac{y}{y^2+\rho^2}+\frac{1}{2\rho^2}\,\frac{1}{\sqrt{\rho^2}}\tan^{-1}\frac{y}{\rho}\right)\Bigg|_{-\infty}^{+\infty}$$

$$=\frac{\sin\theta'-\sin\theta''}{2}$$

To find out if y should be extended to $\pm$ or if a distance somewhat shorter will suffice for an adequate solution we can evaluate the integral for specific values of and y.

So that the $F_{w}t = \frac{1}{\pi} \left(\frac{\sin\theta' - \sin\theta''}{2}\right) \left(\tan^{-1} \frac{y}{\rho} - \tan^{-1} \frac{y}{\rho}\right)$

$$= \left(\frac{\sin\theta' - \sin\theta''}{2}\right) \frac{2 \tan^{-1} y/\rho}{\pi}$$

assume that a 10% reduction in the view factor is maximum acceptable. Then for this expression $\frac{2}{\pi} \tan^{-1} \frac{y}{\rho}$ to have a value of 0.9.

We set $$\frac{2}{\pi} \tan^{-1} \frac{y}{\rho} = 0.9$$

or $$\tan^{-1} \frac{y}{\rho} = 0.45$$

$$= 0.45 \ (180^{o})$$

$$\text{Tan } 81^{o} = \frac{y}{\rho} = 6.3$$

Therefore if ρ = 1000 ft. the y should be $\pm$6300 ft.

It appears therefore that F_{wt} can be evaluated for smaller sections of A_2 without sacrificing much in the way of view factor values.

Appendix "B" Terrain Data used in Calculating the Values of figures
Rogue River Site 1 and Deschutes Site 1

Rogue River Site #1 View Factor $F_{w-t} = 0.213 = 0.21$

14 July 1965 $F_{w-t} = 0.787 = 0.79$

Time of Observation Hours	Water Temp. °F	Air Temp. °F	Ave. Terrain Temp. °F	Vapor Press. in Hg		ENR Net longwave, radiation in ly
0750	72	64	65	.838	.75 to .82	.212
0850	72	74	70	.52		.129
0950	73	84	73	.53		.128
1050	73	88	75	.50		.076
1145	73	96	78	.68		.057
1230	74	100	85	.61		.069
1335	75	99	85	.55		.057
1415	75	97	85	.52		.047
1515	76	95	86			.036
1555	75	94	88			.019
1635	75	96	85			.024
1708	74	95	83			.006
1805	74	84	83			.060

Deschutes Site #1 View Factor $F_{w-t} = 0.14$

29 June 1966 $F_{wa} = 0.86$

Time of Observation Hours	Water Temp. °F	Air Temp. °F	Ave. Terrain Temp. °F	Vapor Pressure in Hg		Time of Observation ENR	ENR Longwave Radiation ly
0800	57	64	75	*	0.75		
					to	0930	.074
0900	58	64	82		0.82	0950	.083
						1015	.072
1000	59	71	89			1030	.059
						1040	.087
1100	60	74	93			1050	.072
						1100	.069
1200	60	75	97			1200	.074
1320	61	77	99			1320	.065
1400	63	82	98			1400	.075
1500	63	81	96			1500	.070
						1615	.075
1600	62	79	89			1625	.076
						1645	.081
1700	62	75	91			1700	.073
						1715	.089
1800	61	73	87			1730	.094
						1750	.095
						1805	.108

* No vapor pressure data due to break down in Cambridge Systems Vapor Mate Instrument responded but data showed values which were impossible. This is very dry country, assume very low vapor pressure.

Appendix "C" Check Calculations for h_a as determined by Analog Model

Case I Observed Conditions:

$$\phi = 45^\circ$$

$$\delta_s = 23^\circ \quad (1 \text{ July})$$

$$\alpha = 0^\circ$$

$$\beta^* = 40^\circ$$

$$h_a(\text{obs.}) = 37.5^\circ \quad \text{(assumed)}$$

1. Calculate $C_3 = \dfrac{1}{\cos \phi \cos \delta_s} = \dfrac{1}{\cos 45^\circ \cos 23^\circ}$

$$= \frac{1}{(.707)(.92)} = 1.536$$

$$C_4 = -\tan \phi \tan \delta_s = \tan 45^\circ \tan 23^\circ$$

$$= -1\ (.424) = -0.424$$

$$\sin h_a = \sin 37.5^\circ = .609$$

$$\cos 0 = 1$$

$$\sin 0 = 0$$

Calculate D $= C_3 \sin h_a + C_4 = 1.536(.609) + (-.424)$

$$= 0.513$$

Square this value -- subtract result from 1 and take square root.

$$D = .513$$

$$D^2 = .264$$

$$1-D^2 = 0.736$$

$$1-D^2 = .858$$

Multiply this result by $\cos \alpha = 1$ $= .858$

Multiply D by $\sin \alpha = 0$ $= 0$

Then $\tan h_a = \tan \beta \left(.858 + 0 \right)$

$= .839 \quad (.858)$

$= .719$

$h_a = 35^\circ 45'$

The next iteration using h_a as the starting value gives the value of $h_a = 36^\circ 25'$

Case II Observed Conditions:

$\phi = 45$

$\delta_s = 13.5$ (Aug. 16)

$\alpha = 60$

$\beta' = 30$

$h_a = 22$ (assumed)

Calculate $C_3 = \frac{1}{\cos\phi \cos\delta_s} = 1.455$

$C_4 = -\tan\phi \tan\delta_s = -.240$

$\sin h_a = \sin 22^\circ = .375$

$C_3 \sin h_a = .53$

$D = C_3 \sin h_a + C_4 = .29$

Square D, Subtract result from 1 and take square root.

$1-D^2 = .958$

Multiply D by $\sin\alpha = .833 \qquad .24$

Multiply $1-D^2$ by $\cos\alpha = .5 \qquad .479$

$\tan h_a = \tan \quad .24 + .479$

$= \tan 40^\circ \quad .719$

$= .577 \ (.719)$

$\tan h_a = .415$

$h_a = 22^\circ 32'$ which is acceptable.

Case III Observed Conditions:

$$\phi = 45$$

$$\delta_s = 17^\circ\ 50'\ \text{(1 Aug)}$$

$$\alpha = 330$$

$$\beta = 30^\circ$$

$$h_a = 23^\circ\ \text{(assumed)}$$

Calculate $C_3 = \dfrac{1}{\cos \phi \cos \delta_s} = 1.485$

$C_4 = -\tan \phi \tan \delta_s = -.313$

$\sin h_a = \sin 23^\circ = .391$

$C_3 \sin h_a = .580$

$D \div C_3 \sin h_a + C_4 = .267$

Square D, Subtract result from 1 and take square-root

$1 - D^2 = .964$

Multiply $1 - D^2$ by $\cos\alpha = .866$

Multiply D by $\sin\alpha = -.500$ and add results.

$\tan h_a = \tan\beta \left[866(.964)+(.267)(-.5)\right]$

$= .577\ (.701)$

$= .4045$

$h_a = 22^\circ$ which is acceptable

Appendix "D" Accumulated Solar Radiation Received at a Horizontal Surface as a Function of Time, [illegible], Latitude and Solar Altitude

The following calculations were made for 1 July for latitudes $\phi = 35^\circ$
16 July $\phi = 45^\circ$
1 Aug. $\phi = 55^\circ$
16 Aug.
1 Sept.
23 Sept.

All functions we rounded off to three significant digits.

Calculation of t_a or sunrise positions in solar path plane

$$\sin h_a = \sin \phi \sin \delta_s + \cos \phi \cos \delta_s \cos t_a$$

Conditions Lat. $\phi = 45^\circ$

Date = 1 June $\quad \delta_{save} = 22^\circ\ 2'$

$h_a = 0$

$0 = \sin 45^\circ \sin 22^\circ\ 2' + \cos 45^\circ \cos 22^\circ\ 2' \cos t_a$

$= (.707)(.375) + (.707)(.927) \cos t_a$

$$\cos t_a = -\frac{.265}{.655}$$

$= -.405$

$t_a = 113^\circ\ 53'$ Line 1, column 4, table 8

The length of solar day (L) rounded off to the nearest 0.1 hour is then

$$L = \left(t_a / 15^\circ\right) 2$$

$$= \left(\frac{113^\circ\ 53'}{15^\circ/\text{hr}}\right) 2$$

$= 15.2$ hours Line 1, column 6, table 8

Calculation of sunrise Azimuth

$$\tan Z = \frac{\sin t}{\cos \phi \tan \delta_s - \sin \phi \cos t}$$

$$= \frac{.914}{(.707)(.405) - (.707)(-.405)}$$

$$= \frac{.915}{.572}$$

$$\tan Z = 1.598$$

$$Z = 57^\circ\ 58'$$

$$Z \cong 58^\circ$$

Calculation of solar altitude at one hour intervals from apparant noon.

$$\sin h = \sin \phi \sin \delta_s + \cos \phi \cos \delta_s \cos t_a$$

where t_a will have the values 0°, 15°, 30°, 45°, 60°, 75°, 90°, 105°, 120°, etc. until sunrise or $h = 0$ is intersected.

These calculations appear in tabular form on the following page.

Date	Lat. degrees	δ degrees	$\sin \phi \sin \delta$	$\cos \phi \cos \delta$	t_a degrees	$\cos t_a$	$\cos \phi \cos \delta \cos t_a$	$\sin h$	h degrees	Rad Int BTU/SF/HR	Ave Rad Int BTU/SF/HR	Accom. Rad received BTU/SF
1 June	43	23° 9'	.265	.633	0	1.000	.633	.920	67.0	253	250	1060
					15	.966	.633	.898	64.0	247	235	810
					30	.866	.567	.832	56.2	222	203	575
					45	.707	.463	.728	46.7	183	162	372
					60	.500	.328	.593	36.4	138	113	210
					75	.259	.170	.435	25.5	88	68	97
					90	.000	.000	.265	16.7	49	27	29
					105	-.259	-.170	.095	5.4	5	2	2
					120	-.500	-.328	-	-	-	-	-
									Plotted in fig. 37 page . as ordinate	from fig.27 page		Plotted in fig. 37 page 37 as abscissa.

Appendix "E" Solar Radiation Blocking by Terrain, Calculations for Deschutes River--Comparison of Sections--Sinomox Quadrangle.

Point No.	Wt. of Section	α	Right Bank				Left Bank			
			β^a	h_a	Solar Radiation Blocked	Weighted Values of Solar Radiation Blocked by Terrain	β^a	h_a	Solar Radiation Blocked	Weighted Values of Solar Radiation Blocked by Terrain
11		81	35.5	10	15		22	5	6.5	
12		51	32	26	81		20.5	15	27.5	
13		20	32.5	32	147		21	20.5	47.5	
14		12.5	29.5	29	110		30	30	121	
15		17	24	24	67		20	20	45	
16		20.5	25	24.5	70		25	19.5	43	
17		287	11.5	4	3		2.5	.5	.5	
18		266	3	.5	.5		22.5	7.5	10.5	
19		6	12	11.5	19		30	29.5	115	
20		9	21	21	50		22.5	22	55	
21		340	22	19.5	43		11.5	10	15	
22		313	30.5	19	41		4	2.5	3	
23		278	20.5	5	6.5		4	.5	.5	
24		78.5	24.5	6	8		13	3.5	4.5	
25		47.5	9	4	4		4	3	4	
26		8	10	16	30.5		6.5	6	8	
27		23	3	3	6.5		23.5	22	55	
28		34.5	7	7.5	10.5		29	27	89	
29		32.5	13	12	20		24	22.5	58	
30		19	17	17	34		5.5	3.5	7	
31		0	18.5	18	37		9.5	9.5	14	
32		300	20	17	34		8	4.5	6	
33		293	20	3	6.5		14	3.5	4.5	
34		18	13	13	22.5		24.5	24.5	70	
35		89.5	9.5	0	0		29.5	.5	.5	
36		314	15	10	15		37	23	61	
37		313	15	10	15		12	8	11.5	
38		201	14	7.5	10.5		12	6	8	
39		54	12.5	10	15		11	8	11.5	
40		0	3	3	6.5		19	19	41	

Sect.	Mt. of Section	α	Right Bank β^*	Right Bank h_a	Right Bank Solar Radiation Blocked	Right Bank Weighted Values of Solar Radiation Blocked by Terrain	Left Bank β^*	Left Bank h_a	Left Bank Solar Radiation Blocked	Left Bank Weighted Values of Solar Radiation Blocked by Terrain
41		312.5	18	12.5	21		13	8.5	12.5	
42		313.5	13	8	11.5		14	9.5	14.5	
43		3	23	22.5	38		12	12	20	
44		60.5	16	7.5	10.5		11	5.5	7	
45		274	13.5	1	1		10.5	2	2.5	
46		273	14	1	1		15.5	4	5	
47		37.5	20	18	37		16	12	20	
48		357	21	20	45		12.5	12	20	
49		359	11	11	17.5		11	11	17.5	
50		10	10.5	10	15		15.5	15	27.5	
51		67	12.5	7	10		16	7.5	10.5	
52		279	9.5	1.5	2		23.5	4.5	6	
53		29	7.5	7.5	10.5		18	17.5	35	
54		70	18.5	8	11.5		9	4	5	
55		14	20.5	20	45		9	9	13	
56		355	15	15	27.5		12	12	20	
57		12	9	9	13		29	29	110	
					1199 /47 = 25.5				1261 /47 = 26.8	

Average Blocked Solar Radiation Right Bank = 25.5 BTU/SF
Average Blocked Solar Radiation Left Bank = 26.8 BTU/SF
Total 52.3 BTU/SF/Day

Sect.	Mt. of Section	α	Right Bank β^*	Right Bank h_a	Right Bank Solar Radiation Blocked	Right Bank Weighted Values of Solar Radiation Blocked by Terrain	Left Bank β^*	Left Bank h_a	Left Bank Solar Radiation Blocked	Left Bank Weighted Values of Solar Radiation Blocked by Terrain
A	2.5	270	22	0	0	0	11	0	0	0
B	3	20	15.5	15	27.5	135	14	14	25	125
C	2	289	13.5	4	5	10	8.5	2	2.5	5
D	3	9	17	17	34	102	12.5	12.5	21	63
E	3	275	14	1	1	3	7.5	.5	.5	2
F	7	31	10.5	10	15	105	19	18	37	259
G	2	290	20	17.5	35	70	13	4.5	6	12
H	1.5	42	10.5	19.5	42	63	22	18	37	55
I	3	307	15	8.5	12	36	14	8	11.5	35
K	2	36	17.5	15	27.5	55	12	11	17.5	35
L	3.5	313	20	13	22	77	9.5	6	8	28
M	3.5	278	13	2	2.5	99	10	2.5	3	12
N	4.5	0	14	14	25	112	6.5	6.5	9	40
O	3	287	7	2	2.5	8	10.5	3	4	12
P	4	355	14.5	14	25	100	11.5	11	17.5	70
	49.5					884 / 49.5 = 17.8				753 / 49.5 = 15.2

Average Blocked Solar Radiation Right Bank = 17.8 BTU/SF
Average Blocked Solar Radiation Left Bank = 15.2 BTU/SF
Total 33.0 BTU/SF/Day

BIBLIOGRAPHY

(1) Gates, David M., "Energy Exchange in the Biosphere, "Harper & Row Biological Monographs. 1962.

(2) Koberg, Gordon E., "Methods to Compute Long-Wave Radiation For the Atmosphere and Reflected Solar Radiation From a Water Surface." Studies of Evaporation, Washington, 1954. (U.S. Geological Survey Professional Paper No. 272 F).

(3) Kreith, Frank. Principles of Heat Transfer. International Textbook Company. 1958.

(4) Monteith, J. L., and Sceicz G., 1961. "The Radiation Balance of Bare Soil and Vegetation." 87(372): 159-170.

(5) Reifsnyder, William E., Lull, Howard W. Radiant Energy in Relation to Forests. Technical Bulletin No. 1344, U. S. Department of Agriculture. December 1965.

(6) Reifsnyder, William E. Applications of Radiation Geometry to Measurement and Interpretation of Radiatn Energy Flux. Yale University, School of Forestry, 28 Sept. - 1 Oct. 1965.

(7) Swan J. B. etal, Economical Radiometer, Performance Construction and Theory. University of Wisconsin Soils Bulletin 4. August 1961.